Proteasome machinery is instrumental in a common gain-of-function program of the p53 missense mutants in cancer

Dawid Walerych[1], Kamil Lisek[1,2], Roberta Sommaggio[3], Silvano Piazza[1], Yari Ciani[1], Emiliano Dalla[1], Katarzyna Rajkowska[1], Katarzyna Gaweda-Walerych[1,4], Eleonora Ingallina[1,2], Claudia Tonelli[5], Marco J. Morelli[6], Angela Amato[7], Vincenzo Eterno[7], Alberto Zambelli[7,8], Antonio Rosato[3,9], Bruno Amati[5,6], Jacek R. Wiśniewski[10] and Giannino Del Sal[1,2,11]

In cancer, the tumour suppressor gene *TP53* undergoes frequent missense mutations that endow mutant p53 proteins with oncogenic properties. Until now, a universal mutant p53 gain-of-function program has not been defined. By means of multi-omics: proteome, DNA interactome (chromatin immunoprecipitation followed by sequencing) and transcriptome (RNA sequencing/microarray) analyses, we identified the proteasome machinery as a common target of p53 missense mutants. The mutant p53–proteasome axis globally affects protein homeostasis, inhibiting multiple tumour-suppressive pathways, including the anti-oncogenic KSRP–microRNA pathway. In cancer cells, p53 missense mutants cooperate with Nrf2 (NFE2L2) to activate proteasome gene transcription, resulting in resistance to the proteasome inhibitor carfilzomib. Combining the mutant p53-inactivating agent APR-246 (PRIMA-1MET) with the proteasome inhibitor carfilzomib is effective in overcoming chemoresistance in triple-negative breast cancer cells, creating a therapeutic opportunity for treatment of solid tumours and metastasis with mutant p53.

The majority of mutant p53 proteins in human cancer cells are a result of missense mutations of the *TP53* tumour suppressor gene, which are among the most frequent genetic events in human tumours[1]. Apart from inactivating wild-type p53 functions, they endow p53 mutants with oncogenic gain-of-function (GOF) properties[2–9]. The GOF p53 mutants are mostly known to impact on tumour cell biology by significantly altering gene transcription[10,11].

However, understanding of the impact of p53 mutants in different cell backgrounds is limited, including the extent of their transcription-dependent and -independent control over a protein content of cancer cells. Moreover, the question has remained poorly addressed as to whether the tumour-promoting GOF mechanisms rely on the acquisition of specific properties linked to each point mutation and interplay with diverse cell backgrounds, or on a pool of common targets—a 'core' GOF program—under the control of multiple p53 mutant proteins in various tumour models.

Here we report the identification of the proteasome machinery as a major common target of five p53 missense variants in a mutant *TP53*-enriched breast cancer subtype—triple-negative breast cancer (TNBC)[12,13], which we validated in other cancer types.

In cancer, increased 20S/26S proteasome and immunoproteasome activity results in a ubiquitin-dependent and -independent degradation of tumour suppressor proteins[14,15]. The proteasome inhibitors bortezomib and carfilzomib are clinically approved for the treatment of multiple myeloma[16]. Although a number of studies support a therapeutic potential of the proteasome inhibitors in solid tumours[17,18], the described resistance mechanisms have not allowed these therapies to progress beyond clinical trials[19].

We report here a key role of the p53 missense mutants in the resistance of TNBC cells to the proteasome inhibitor carfilzomib. We provide evidence that the GOF p53 mutants co-opt the transcription factor Nrf2 to upregulate the proteasome and induce a 'bounce-back'

[1]Laboratorio Nazionale CIB, Area Science Park Padriciano, Trieste 34149, Italy. [2]Dipartimento di Scienze della Vita-Università degli Studi di Trieste, Trieste 34127, Italy. [3]Department of Surgery, Oncology and Gastroenterology, University of Padova, Padova 35128, Italy. [4]Laboratory of Neurogenetics, Mossakowski Medical Research Centre, Polish Academy of Sciences, Warsaw 02106, Poland. [5]Department of Experimental Oncology, European Institute of Oncology (IEO), Milan 20141, Italy. [6]Center for Genomic Science of IIT@SEMM, Fondazione Istituto Italiano di Tecnologia (IIT), Milan 20139, Italy. [7]Laboratory of Experimental Oncology and Pharmacogenomics, IRCCS 'Salvatore Maugeri' Foundation, Pavia 27100, Italy. [8]Unit of Medical Oncology, Azienda Ospedaliera Papa Giovanni XXIII, Bergamo 24127, Italy. [9]Istituto Oncologico Veneto IOV-IRCCS, Padova 35128, Italy. [10]Biochemical Proteomics Group, Department of Proteomics and Signal Transduction, Max Planck Institute of Biochemistry, Martinsried D82152, Germany.
[11]Correspondence should be addressed to G.D.S. (e-mail: delsal@lncib.it)

Accepted 25 May 2016

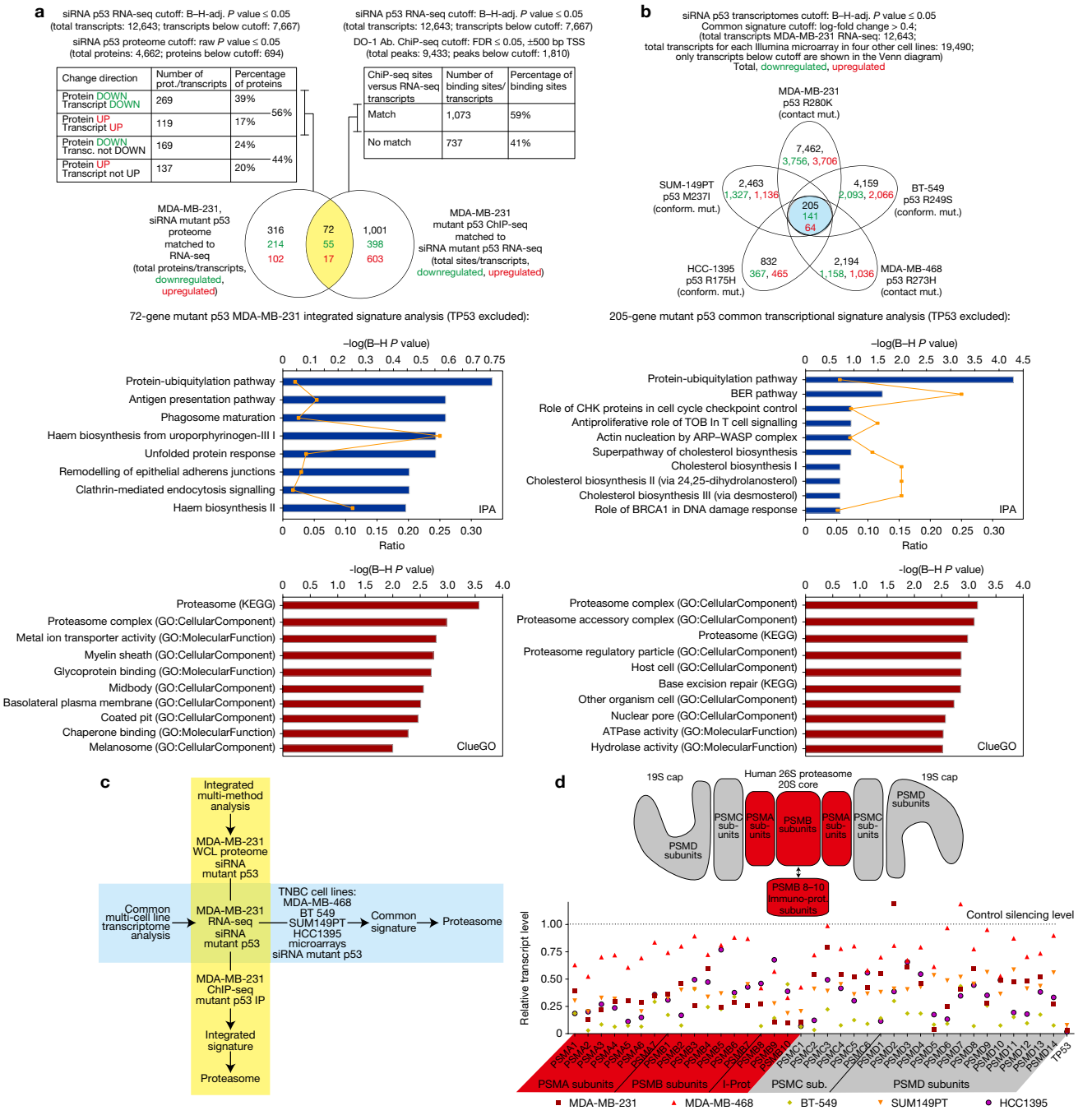

Figure 1 The proteasome is the most affected and conserved pathway controlled by missense mutant p53 variants in TNBC cell lines. (**a**) An integrated analysis of the mutant p53 program in MDA-MB-231 cells. The top left table shows matching of the proteomic and RNA-sequencing (RNA-seq) data on mutant *TP53* silencing (proteomics: $n=4$ biologically independent samples for each condition, raw P value $P \leq 0.05$; RNA-seq: $n=3$ biologically independent samples for each condition, B–H-adj. P value $P \leq 0.05$). The top right table shows the match of chromatin immunoprecipitation followed by sequencing (ChIP-seq) peaks (DO-1 immunoprecipitation, cutoff for called peaks: FDR $\leq$ 0.05, $\pm$500 bp of the adjacent TSS) to RNA-seq transcriptomic data on mutant *TP53* silencing ($n=3$ biologically independent samples for each condition, B–H-adj. P value $P \leq 0.05$). Transcripts in agreement with protein level changes and ChIP-seq peaks (both in majority) are overlapped in the Venn diagram, resulting in an integrated 72-gene signature. The signature is analysed by the pathway association: IPA pathways (top graph: bars—log(B–H-adjusted P values of the pathway association), line—ratios of the number of found genes to the total number of genes in the pathways) and ClueGO (bottom table; bars—log(B–H-adjusted P values of the GO-term/pathway association)). Additional results are in Supplementary Fig. 1 and Supplementary Tables 1–4, and 13. (**b**) Venn diagram of the multi-transcriptome analysis performed in the indicated five TNBC cell lines with indication of the silenced *TP53* mutants ($n=3$ biologically independent samples for each cell line and condition, B–H-adj. P value $P \leq 0.05$) and the 205-gene common signature pathway association results, as in **a**. Additional results are in Supplementary Fig. 1 and Supplementary Tables 3 and 13. (**c**) Scheme of the used multi-omic mutant p53 GOF high-throughput analyses performed in the TNBC cell lines presented in **a**,**b**. (**d**) Levels of human 26S proteasome and immunoproteasome (shown schematically in the top picture) subunit gene transcripts in the five TNBC cell lines (as in **b**) on mutant *TP53* silencing (each result is a mean of two independent experiments). Additional results are in Supplementary Fig. 1 and Supplementary Table 5. Statistics source data for **d** are provided in Supplementary Table 10.

recovery of proteasome gene expression following inhibitor administration. On the basis of these findings, we simultaneously targeted p53 mutants and their downstream pathway—the proteasome—in TNBC cells, overcoming resistance to pharmacological inhibition of the proteasome.

RESULTS

Proteasome pathway is a common transcriptional target of various p53 missense mutants in TNBC cells

To gain novel insights into the oncogenic GOF of mutant p53 in cancer cells, we first used a combination of large-scale approaches in the MDA-MB-231 cells (Fig. 1a,c)—a TNBC cellular model, whose transformed phenotype relies on the high level of a R280K mutant variant of p53[6,8]. As shown in Fig. 1a, we observed on silencing of mutant *TP53* that 56% of the significantly up- and downregulated proteins identified by a differential whole-cell proteome analysis[20,21] (Supplementary Table 2) match their corresponding transcripts, identified by RNA sequencing (Supplementary Table 3). In parallel (Fig. 1a), on silencing of mutant *TP53*, we observed significant changes in the levels of transcripts for the 59% of corresponding transcription start sites that were identified by mutant p53 in ChIP-sequencing analysis (±500 bp from adjacent transcription start sites (TSSs); Supplementary Table 4). These results suggested that in MDA-MB-231 cells the majority of the observed mutant p53-dependent protein changes are related to its transcriptional activity and that binding of mutant p53 to the majority of gene promoters in the proximity of TSSs results in a significant modulation of transcription at the corresponding loci. Overlapping the lists of transcripts matched to the corresponding proteins and transcripts matched to the mutant p53-bound TSS regions, we obtained a 72-gene integrated signature. Pathway and GO-term enrichment analysis of the integrated signature suggested the proteasome-ubiquitylation pathway to be the most affected process (Fig. 1a).

Having demonstrated that the transcriptional activity is pivotal to the R280K mutant p53 GOF in the MDA-MB-231 cell line, we decided to focus our attention on mutant p53-regulated transcriptomes. The MDA-MB-231 transcriptome has been compared with mutant p53 messenger RNA profiles obtained from four other TNBC cell lines carrying contact or conformational missense mutations of *TP53*[22], on mutant *TP53* silencing (Fig. 1b,c and Supplementary Tables 3 and 12). Strikingly, the 205-gene common signature, just like the integrated signature obtained from MDA-MB-231 cells, was most significantly enriched with genes belonging to the proteasome-ubiquitylation pathway (Fig. 1b). Notably, among the WT p53 targets identified in recent transcriptomic and ChIP-seq studies carried out in various cell models there are no proteasome-ubiquitylation pathway genes shared with our integrated or common mutant p53 signatures[23–26].

Both integrated and common mutant p53 signatures contain multiple 26S proteasome and immunoproteasome subunit genes (Supplementary Tables 1 and 13). To clarify and validate these data, we quantified the mRNA levels for all 37 proteasome and immunoproteasome subunit genes expressed in humans, in the 5 TNBC cell lines of interest. Transcription of a great majority of the genes was downregulated on the mutant *TP53* knockdown (Fig. 1d and Supplementary Fig. 1e and Supplementary Table 5), accompanied by a downregulation of the corresponding proteins (Supplementary Fig. 3a).

Silencing-rescue experiments in MDA-MB-231 cells demonstrated that the five full-length mutant p53 variants derived from the panel of TNBC cell lines of interest are interchangeable with respect to their ability to upregulate the expression of ten proteasome genes that represent all of the proteasome components (Supplementary Fig. 3b). This evidence confirms that proteasome-machinery-encoding genes are targets shared by different p53 missense mutants within a common transcriptional program.

The proteasome expression signature is strongly associated with poor prognosis and mutant status of *TP53* in cancer patients

We next explored association between expression levels of the identified mutant p53-related gene sets, prognosis in cancer patients' data sets or presence of mutant *TP53* in clinical samples.

The mutant p53 common signature, derived from the panel of TNBC cell lines, showed more significant association with a poor prognosis in breast cancer than any mutant p53 signature derived from the five TNBC cell lines individually (Fig. 2a and Supplementary Table 1). This result suggests that in breast cancer, the most significantly oncogenic GOF transcriptional program is shared between different p53 mutants and cell backgrounds rather than being associated with the individual mutants in their cellular contexts. Strikingly, high expression of the whole proteasome 37-gene signature was able to more effectively discriminate a poor outcome of the patients than the mutant p53 common signature and other top pathway signatures or signatures derived from the individual TNBC cell lines (Fig. 2a and Supplementary Fig. 2a).

Since all 37 proteasome genes are upregulated by mutant p53 (Fig. 1d), we decided to test the association between the mutational status of *TP53* and this signature in breast cancer. As a control, we also analysed an equal number of upregulated genes in common and cell line-specific signatures and used the Pearson's χ^2 test to verify whether the mutant status of *TP53* and the expression of the signatures are independent (Fig. 2b). Also in this case, the high expression of the 37-gene whole proteasome signature was most strongly associated with the *TP53* mutations, with the highest χ^2 test value (Fig. 2b). We also found a positive association between the high expression level of the 37-gene whole proteasome signature and the presence of mutant *TP53* in the data sets of patients with cancers of head and neck, lung, pancreas, bladder, colon, brain, stomach and liver (Supplementary Fig. 2d).

This implies that the whole proteasome overexpression is a conserved effect of the missense *TP53* mutation presence in various cancer types.

Mutant p53 proteins increase the activity of the proteasome machinery in *in vitro* and *in vivo* cancer models

In line with expression data, depletion of mutant p53 in the TNBC cell lines, but not WT p53 in MCF7 breast cancer cells or MCF10A—non-transformed breast epithelium cells, resulted in a significant decrease of proteasome rate-limiting chymotrypsin-like (Fig. 3a) and trypsin-like activities (Supplementary Fig. 3c). As a positive control of the proteasome downregulation we used silencing of the essential proteasome gene *PSMA2* and two clinically approved proteasome inhibitors—bortezomib and carfilzomib.

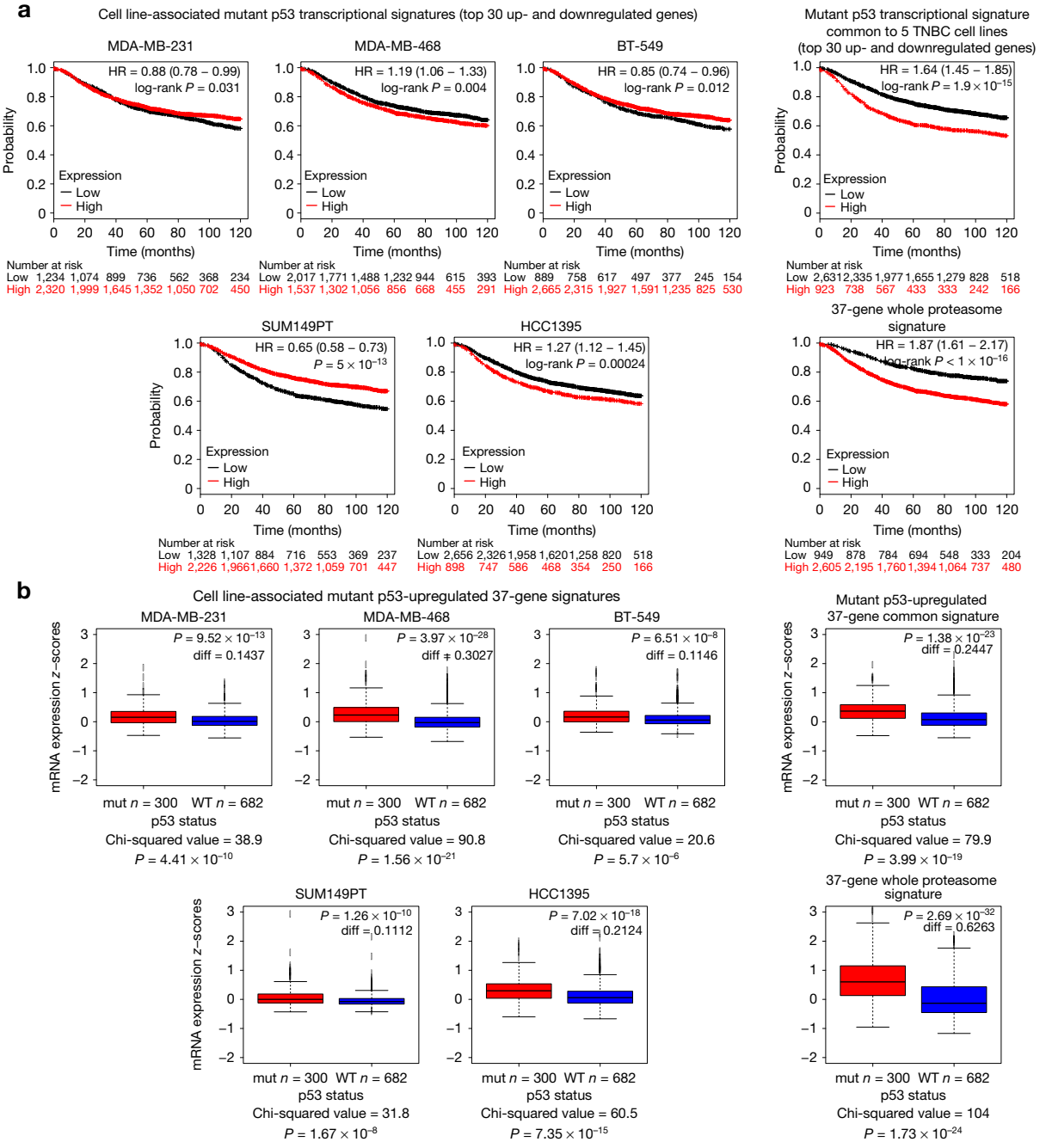

Figure 2 The proteasome expression signature is associated with a poor patient prognosis and a mutant *TP53* status in breast cancer. (**a**) Association of the mutant p53-related signatures derived from the indicated TNBC cell lines, the mutant p53-related 205-gene common signature and the 37-gene, 'whole proteasome signature' with the survival of breast cancer patients. The red curve ('high') represents the transcript levels in patients matching the level in the presence of mutant p53 in the cell line-derived signature, black curve ('low')—expression level not matching the presence of mutant p53 (top 30 genes downregulated and top 30 genes upregulated were used; see Methods for analysis details). HR—hazard ratio; log-rank P—log-rank test *P* value for the curves comparison. Numbers below graphs indicate number of patients at risk—total and at consecutive time points; $n=3{,}458$—meta-data set composed of 3,458 samples associated with the Km-plotter online analysis tool. (**b**) Association of the mutant/WT *TP53* status with expression of the indicated 37 genes in breast carcinoma—genes derived from each cell line individually (top plots), genes derived from the common 205-gene transcriptional signature or the 37-gene whole proteasome and immunoproteasome signature (bottom plots). The signatures used here were all 37 genes and contain only genes upregulated by mutant p53 to allow a direct comparison with the 37-gene whole proteasome signature—which is composed of proteasome subunit genes upregulated by mutant p53. Box plots: diff—difference in mean gene expression in mutant versus WT p53 status samples; *P* value is derived from Mann–Whitney *U*-test ($n=982$). Below each plot the independence chi-squared (χ^2) test value (degrees of freedom = 1) along with the supporting *P* value is shown. The χ^2 test indicates whether the mutant p53 status is independent of a high expression of a signature—the higher the value and the lower the *P* value the less probable the independence. Centre represents the median, box extremes indicate the first and third quartiles, and whiskers extend to the extreme values included in the interval calculated as ±1.58 IQR/sqrt(*n*), where the IQR (interquartile range) is calculated as the third quartile minus the first quartile. Additional results are shown in Supplementary Fig. 2.

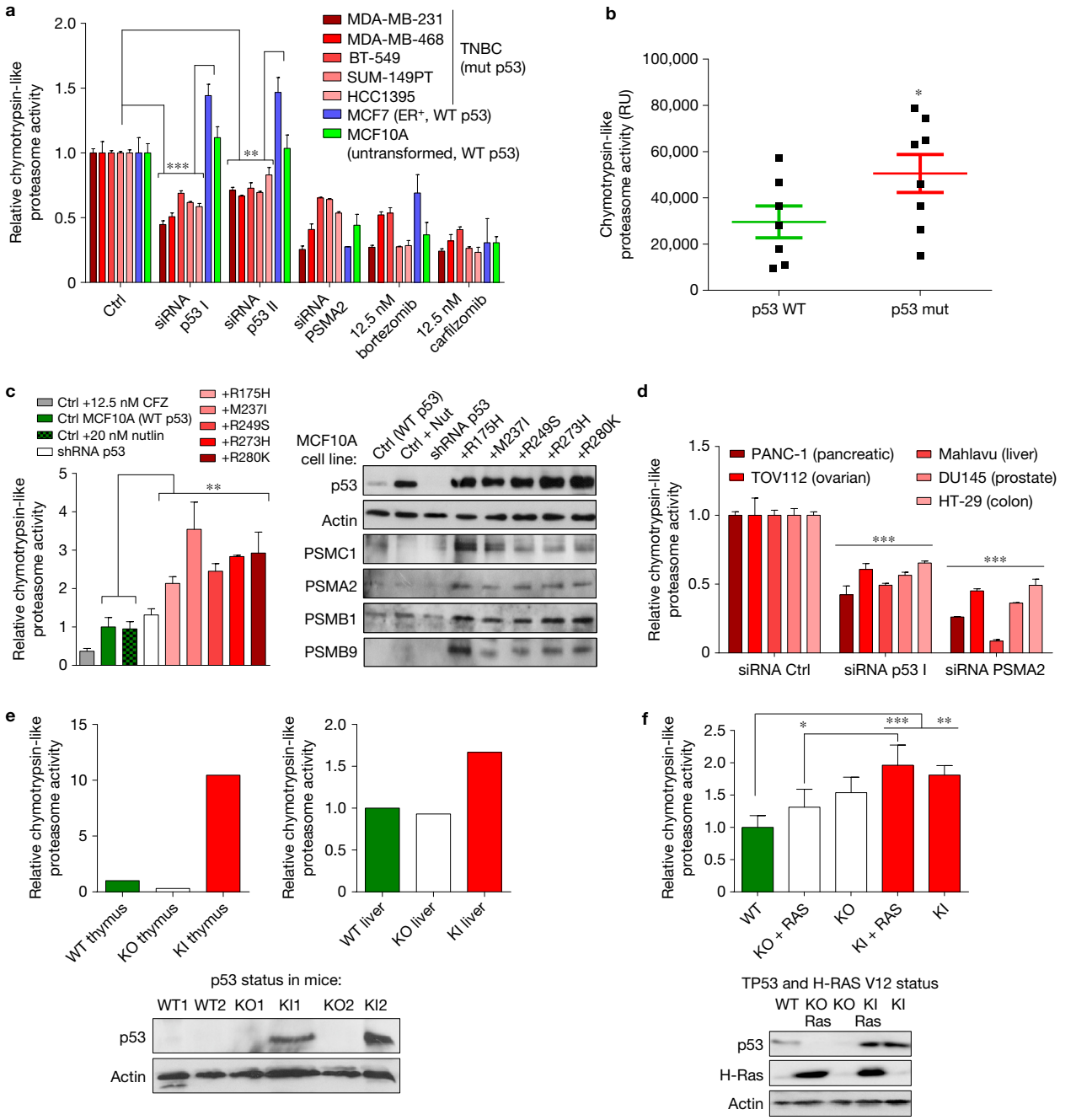

Figure 3 The proteasome activity is elevated in the presence of the GOF p53 mutants in various cancer models. (**a**) Chymotrypsin-like proteasome activity in five mutant (mut) p53 TNBC cell lines versus two WT p53 cell lines (MCF10A and MCF7) on silencing of mutant *TP53* or *PSMA2* or proteasome inhibitor treatment (24 h; carfilzomib, bortezomib). (**b**) Chymotrypsin-like proteasome activity in human basal-like breast cancer primary tumours is on average elevated in the missense mutant *TP53* tumours compared with the wild-type tumours ($n=8$ versus $n=7$ biologically independent tumour samples). Means with s.e.m. are shown; *t*-test, $^{*}P<0.05$. (Additional results are in Supplementary Fig. 3d.) (**c**) Chymotrypsin-like proteasome activity in MCF10A cell lines stably transfected with empty retroviral vector (Ctrl), vector encoding shRNA targeting *TP53* (shRNA p53) and indicated mutant p53 cds shRNA-resistant HA-tagged variants, stably introduced into the MCF10A shRNA p53 cell line (+p53 changed residue). Ctrl MCF10A cells were also treated with 20 μM nutlin for 24 h to induce WT p53 accumulation. CFZ, carfilzomib. Right: western blot with p53 and indicated proteasome subunit levels in the MCF10A-derived cell lines. (**d**) Chymotrypsin-like proteasome activity in the non-breast cancer cell lines with p53 missense mutants is decreased on silencing of mutant *TP53* expression or of *PSMA2* proteasome subunit expression. (**e**) Chymotrypsin-like proteasome activity is elevated in protein extracts from thymuses (enlarged with lymphomas in KO/KI mice) and livers (infiltrated with lymphoma cells in KO/KI mice) mice with the KI R172H p53 genotype as compared with the WT/KO genotype mice (2 mice for each genotype). Bottom: p53 protein levels in liver extracts (western blot). (**f**) Chymotrypsin-like proteasome activity is elevated in MEFs from mice with the KI R172H *TP53* genotype as compared with the activity observed in MEFs from WT/KO genotype mice, with or without a stable overexpression of the *HRAS* V12 oncogenic variant. Bottom: corresponding western blot with p53 and Ras level detection. (**a**,**c**,**d**,**f**) Means of $n=3$ biologically independent samples with s.d. are shown, ANOVA test with Bonferroni correction: $^{*}P<0.05$, $^{**}P<0.01$, $^{***}P<0.001$. Additional results are shown in Supplementary Fig. 3. Unprocessed original scans of blots are shown in Supplementary Fig. 9. Statistics source data for **a**,**c**–**f** are provided in Supplementary Table 10.

In frozen primary tumour samples obtained from 15 basal-like breast cancer patients (including 10 TNBCs), the presence of the elevated proteasome activity correlated with the presence of p53 missense mutants determined by *TP53* mRNA sequencing and immunohistochemical staining (Fig. 3b and Supplementary Fig. 3d).

Expression of each of the *TP53* mutant variants, characterizing the five TNBC cell lines, in MCF10A cells with depleted endogenous WT p53, caused a significant increase of the proteasome activity, protein and transcript levels of selected proteasome subunits (Fig. 3c and Supplementary Fig. 3e,f). Importantly, we observed a significant decrease in proteasome activity and in proteasome subunit transcription following mutant *TP53* silencing in other cancer-derived cell lines—hepatic, ovarian, pancreatic, prostatic and colonic—carrying various GOF p53 mutants (Fig. 3d and Supplementary Fig. 3h).

In line with the above observations, proteasome activity was significantly increased in thymic lymphomas and lymphoma-infiltrated enlarged livers derived from mutant *TP53* knock-in mice expressing p53 variant R172H (Fig. 3e). These organs were chosen for comparative analysis in mouse models since their transformation-related changes are pathologically comparable in mutant *TP53* R172H KI and *TP53* KO mice[27]. Also in mouse embryo fibroblasts (MEFs) derived from the same mice the elevated proteasome activity correlated with the mutant *TP53* KI status and the effect was enhanced by an overexpression of the oncogenic *RAS* V12 variant (Fig. 3f).

These *in vitro* and *in vivo* findings strongly support the dependence of proteasome activity on the presence of the p53 mutants in different cancer types.

Nrf2 transcription factor cooperates with GOF p53 mutants in binding the 26S proteasome subunit gene promoters

To investigate the molecular mechanism underlying the proteasome transcriptional regulation by the p53 mutants in cancer, we analysed the ChIP-sequencing data obtained from the MDA-MB-231 cell line (Fig. 1a and Supplementary Table 4). We defined candidate mutant p53-binding regions within promoters of ten genes encoding proteasome subunits, selected to represent all proteasome functional parts, and confirmed binding of mutant p53 to all these regions in the five TNBC cell lines of interest (Fig. 4a and Supplementary Table 4).

We next performed a bioinformatics analysis to identify consensus sequences significantly enriched in the mutant p53-bound regions in all 37 proteasome genes. We found that the most frequently represented sequence motifs match the binding sites of known transcription factors, with no indication of the WT p53 consensus binding site (Supplementary Table 6). These included motifs for Nrf1 (NFE2L1/TCF11), Nrf2 (NFE2L2), STAT3, NF-YA, NF-κB (Fig. 4b) that have been previously reported to control basal transcription of 26S proteasome and immunoproteasome genes[28–31], the last two having been reported to cooperate with mutant p53[3,32] (Fig. 4b). We silenced the expression of these factors in MDA-MB-231 cells to investigate their impact on activity and transcription of the proteasome (Supplementary Fig. 4b). Only silencing of *NRF1* or *NRF2* resulted in downregulation of *PSMA2* and *PSMC1* transcription (selected as 26S proteasome representative genes) and proteasome activity to the levels comparable to the mutant *TP53* silencing (Fig. 4c). Double knockdown experiments suggested that the effect of Nrf1 is additive and as such independent of mutant p53, while the activities of Nrf2 and mutant p53 are not additive and possibly interdependent (Fig. 4d).

Indeed, ChIP analysis confirmed that recruitment of mutant p53 to *PSMA2* and *PSMC1* gene promoters relies on the presence of Nrf2 but not Nrf1, while Nrf2 binding weakly depends on mutant p53 (Fig. 4e). In MDA-MB-231 cells, mutant p53 and Nrf2 increase the recruitment of the acetyltransferase p300 at *PSMA2* and *PSMC1* promoters more strongly than Nrf1 and induce the p300-dependent acetylation of histone 3 Lys9 at these loci (Fig. 4f,g)—a marker of transcriptionally active chromatin[33]. Conversely, WT p53 does not bind to the proteasome gene promoters in MCF7 cells (Supplementary Fig. 4d).

These data indicate that mutant p53 is specifically recruited to the proteasome gene promoters by Nrf2. Together with the fact that silencing of *NRF2* in MDA-MB-231 cells significantly downregulated transcription of most subunits of the whole proteasome machinery (Supplementary Fig. 4e) our results suggested that the transcriptional control of mutant p53 over proteasome subunit genes is dependent on Nrf2.

Nrf2 interacts with p53 mutants but not with wild-type p53 and is required for the mutant p53-mediated transactivation of the proteasome genes

To deepen our understanding of the interplay between p53 mutants and Nrf2 in regulating proteasome gene transcription, we evaluated their ability to interact. Co-immunoprecipitation experiments revealed that the endogenous Nrf2 protein, in contrast with other tested transcription factors, interacts with the p53 missense mutants in all tested TNBC cells but not with endogenous WT p53 in MCF7 and MCF10A cells (Fig. 5a and Supplementary Fig. 5a). Interestingly, this interaction was abolished on treatment of MDA-MB-231 cells with PRIMA-1 (Fig. 5b), a drug that binds and converts mutant p53 into a wild-type-like, active protein[34].

We confirmed that in the MDA-MB-231 cell line Nrf2 co-localizes in the nucleus with mutant p53, with or without the oxidative stress that induces Nrf2 translocation to the nucleus (Supplementary Fig. 5e,h)[35], and that the interaction of both proteins occurs in the nuclear fraction of these cells (Supplementary Fig. 5f). Furthermore *NRF2* or *TP53* silencing reduces the mRNA levels of the proteasome genes in both control and oxidative stress conditions, while *TP53* silencing has an opposite effect on the expression of the oxidative stress response gene *HMOX1* (HO-1), as described earlier[36] (Supplementary Fig. 5g).

The presence of the stably overexpressed mutant p53 variants (R280K or R175H) in MCF10A cells resulted in a detectable mutant p53–Nrf2 interaction, while WT p53, even accumulated on nutlin treatment, did not interact with Nrf2 (Fig. 5c; for co-localization see Supplementary Fig. 5i). In these cells, mutant p53-induced expression of *PSMA2* and *PSMC1* was significantly downregulated by the *NRF2* or *TP53* silencing (Fig. 5d). We found the same interaction and regulation pattern in H1299 lung carcinoma cells (p53-null) on p53 overexpression (Supplementary Fig. 5b,d). In H1299 cells we mapped the interaction of mutant p53 with Nrf2 to the DNA-binding domain of p53 mutants (Supplementary Fig. 5c).

These data indicate that the mutant p53–Nrf2 interaction is conserved in all of the tested mutant variants and cellular environments,

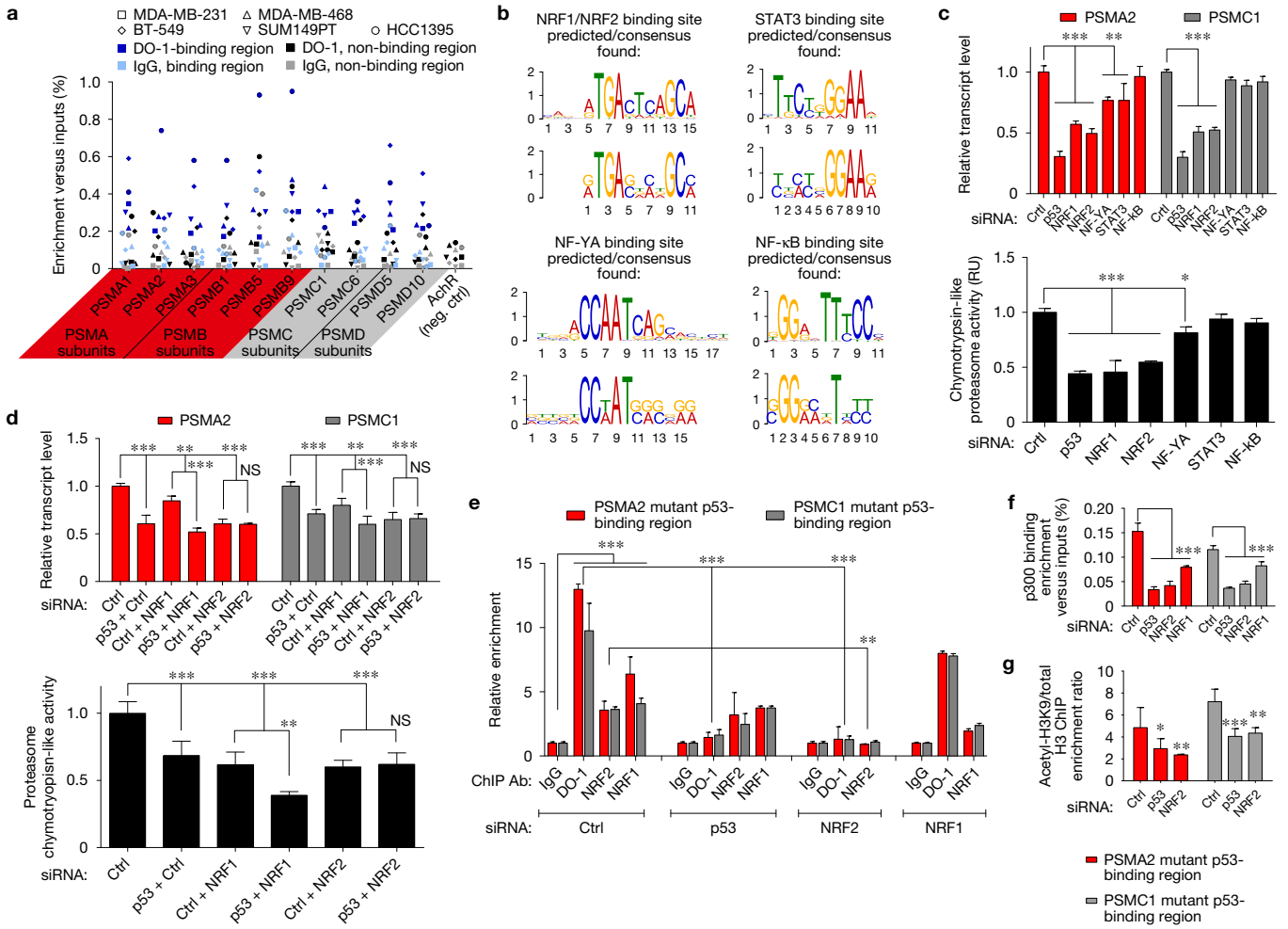

Figure 4 Mutant p53 cooperates with Nrf2 in binding and activating promoters of the 26S proteasome subunit genes. (**a**) ChIP is enriched in anti-p53 DO-1 antibody IP in the mutant p53-binding regions (defined in Supplementary Fig. 4a on the basis of the ChIP-seq result) but not in the p53 non-binding ChIP-seq-defined regions or the IP with a control IgG antibody. A heterochromatic *AchR* locus was used as a ChIP negative control. Results for the panel of five TNBC cell lines are shown (each result is a mean of two independent experiments). For ChIP qPCR values for each region see Supplementary Table 4. (**b**) Predicted (upper) and derived (lower) consensus sequence motifs in the mutant p53-binding regions of the proteasome genes. These motifs correspond to the binding sites of the transcription factors known to be involved in the regulation of proteasome gene expression: Nrf1 (NFE2L1), Nrf2 (NFE2L2), NFYA, STAT3, NF-κB. For a full list of transcription factor motifs and number of sites found in the mutant p53-binding regions, see Supplementary Table 6. (**c**) Transcription levels of *PSMA2* and *PSMC1* proteasome genes (top graph) and chymotrypsin-like proteasome activity (bottom graph) on silencing of mutant *TP53* and candidate mutant p53 transcription cofactors (*NRF1/2, NFYA, STAT3, NFKB1*). (**d**) As in **c**, on double silencing of mutant p53 and *NRF1/2* transcription factors. (**e**) ChIP of mutant p53-binding regions of the *PSMA2* and *PSMC1* genes with the indicated antibodies (Ab) on siRNA-mediated silencing of mutant *TP53*, *NRF2* or *NRF1*. (**f**) ChIP enrichments obtained with anti-p300 antibody at mutant p53-binding regions of *PSMA2* and *PSMC1* genes in MDA-MB-231 cells on treatment with the indicated siRNAs. (**g**) Ratios of ChIP enrichments obtained with anti-acetyl-histone H3K9 (Lys9) antibody and anti-histone H3 antibody, indicating the proportion of acetylated histone H3 at *PSMA2* and *PSMC1* mutant p53-binding regions in MDA-MB-231 cells on treatment with the indicated siRNAs. **c**–**g** show means of $n=3$ biologically independent samples with s.d., ANOVA test with Bonferroni correction: $^{*}P<0.05$, $^{**}P<0.01$, $^{***}P<0.001$; additional results are shown in Supplementary Fig. 4. NS, not significant. Statistics source data for **a**,**d**–**g** are provided in Supplementary Table 10.

and Nrf2 presence is required for the mutant p53-dependent stimulation of the proteasome transcription.

The mutant p53–proteasome axis destabilizes a miRNA maturation factor KSRP to induce aggressive phenotype in TNBC cells

We expected that mutant p53-dependent regulation of the proteasome activity should impact on the proteome of cancer cells and their transformed phenotype. This assumption is supported by our proteomic analysis of MDA-MB-231 cells, showing that 20% of all proteins significantly changing their levels on silencing of mutant *TP53* are upregulated without significant increase of the corresponding transcripts while 17% of the changing proteins do match the upregulated transcripts (Fig. 1a). These findings imply that the suppression of protein levels by mutant p53 in MDA-MB-231 cells is exerted in majority via transcript level-independent mechanisms.

To investigate which proteins are targets of the proteasome machinery, the proteins that were significantly upregulated in

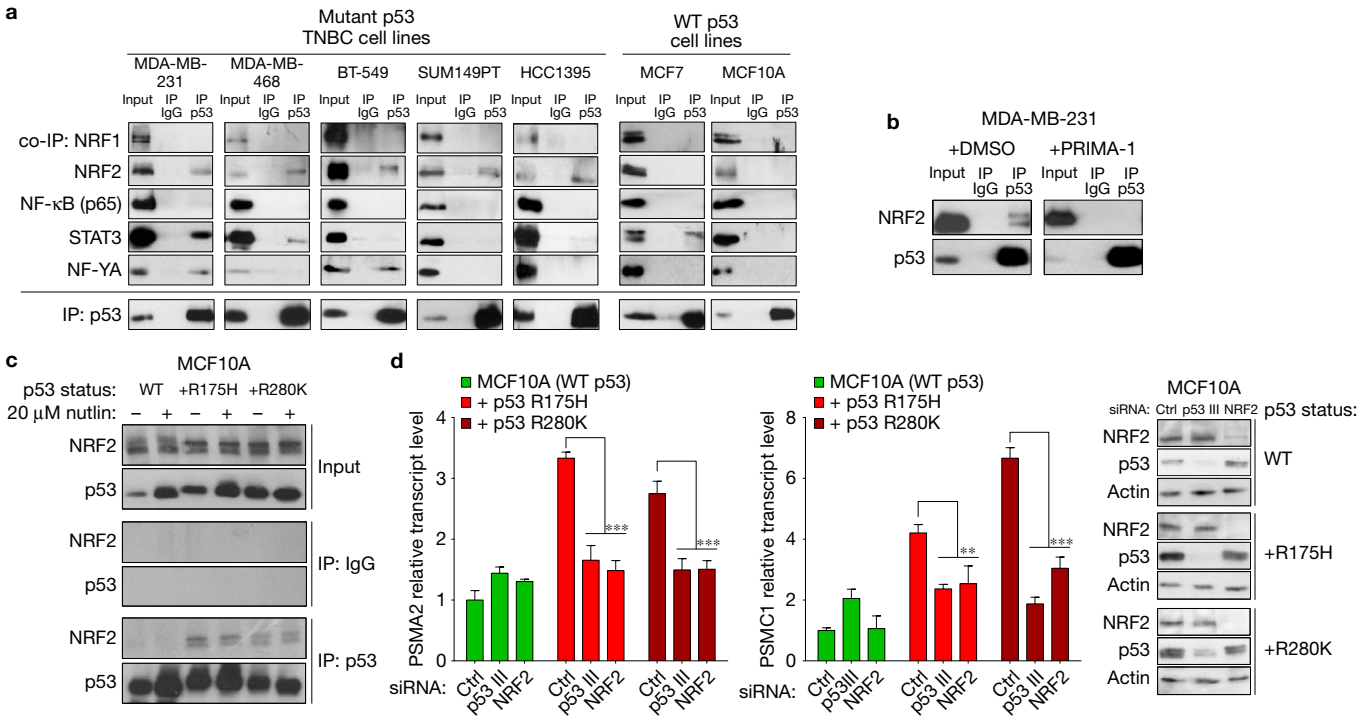

Figure 5 The GOF p53 mutants interact with Nrf2 and are functionally sensitive to *NRF2* silencing. (**a**) Western blot result of co-immunoprecipitation of mutant p53 (DO-1 antibody) with the candidate mutant p53 transcription cofactors (Nrf1, Nrf2, NFYA, STAT3, NFκB-p65) in lysates from the indicated five TNBC mutant p53 cell lines and two WT p53 cell lines (representative of two repeats). (**b**) Western blot result of co-immunoprecipitation of mutant p53 (DO-1 antibody) with Nrf2 after 24 h treatment of MDA-MB-231 cells with dimethylsulfoxide (DMSO) or 1 μM PRIMA-1 (representative of three repeats). (**c**) Co-immunoprecipitation (DO-1 or IgG antibody) of p53 and Nrf2 is shown in control or p53-stabilizing conditions (24 h 20 μM nutlin treatment) for normal MCF10A cells with endogenous WT p53 (WT) and in the mutant p53-overexpressing MCF10A cells with stably silenced endogenous WT p53 (+p53 R175H and +p53 R280K). Representative of three repeats. (**d**) *PSMA2* or *PSMC1* gene expression in MCF10A cells (control cells or cells with stably silenced endogenous WT p53 and introduced mutant p53 variants +p53 R175H or +p53 R280K) on indicated silencing (Ctrl, *NRF2*, p53 III; for *TP53* silencing the siRNA was used that targets p53 cds outside the residues used to produce siRNA resistance for the p53 I sequence). Means of $n = 3$ biologically independent samples with s.d. are shown, ANOVA test with Bonferroni correction: $^{**}P < 0.01$, $^{***}P < 0.001$. The protein levels were controlled in the western blot (right, representative of two repeats). Additional results are shown in Supplementary Fig. 5. Unprocessed original scans of blots are shown in Supplementary Fig. 9. Statistics source data for **d** are provided in Supplementary Table 10.

MDA-MB-231 on *TP53* knockdown, with no match to the respective transcripts, were compared with those significantly upregulated in the whole-cell lysate proteomic analysis on knockdown of the essential proteasome subunit gene *PSMA2* (Fig. 6a and Supplementary Table 2). Twenty-nine proteins were found to overlap and were hence considered as the strongest candidates for degradation coordinated by the mutant p53–proteasome axis (Fig. 6a,b and Supplementary Table 1).

These proteins were analysed *in silico* and two main functional clusters, related to RNA maintenance and to mitochondrial metabolism, were identified (Fig. 6b). In each cluster, we have selected two candidates that possess a tumour-suppressing potential—marked red in Fig. 6b—*KHSRP* (KSRP)[37], *SFRS11*[38], *SUCLA2*[39], *TSFM* (EFTs)[40]. We tested the effects of their silencing in MDA-MB-231 cells on phenotypic outcomes shared by mutant p53 and proteasome downregulation: viability decrease, reduction in migration and chemoresistance (Fig. 6c–e). To address the impact on chemoresistance, we used the proteasome inhibitor carfilzomib (Fig. 3a). For comparison we silenced the expression of tumour suppressors well known to be targets of the proteasome—*CDKN1A* (p21), *CDKN1B* (p27) (cell cycle suppressors), *BCC3* (PUMA) and *PMAIP1* (NOXA) (apoptosis activators)[14] (Supplementary Fig. 6d). Interestingly, KSRP was the only protein whose depletion significantly rescued all of the three tested phenotypic effects observed on silencing of mutant *TP53* or *PSMA2* (Fig. 6c–e). We confirmed that KSRP is stabilized and accumulates on mutant *TP53* or *PSMA2* silencing in MDA-MB-231 and other TNBC cell lines (Fig. 6f,g and Supplementary Fig. 6b,g), while mutant p53 and KSRP do not interact in MDA-MB-231 cells (Supplementary Fig. 6c).

Mutant *TP53* or *PSMA2* silencing also resulted in the elevation of the tumour-suppressive miRNAs let-7a and miR-30c, whose maturation is dependent on KSRP function[37] (Fig. 6h,i and Supplementary Fig. 6h). Conversely, the *KHSRP* silencing and double silencing of *KHSRP* with either mutant *TP53* or *PSMA2* resulted in low levels of the aforementioned miRNAs, indicating a role of mutant p53 in their downregulation through the proteasome-dependent destabilization of KSRP (Fig. 6h,i).

These results highlight a key route of the mutant p53–proteasome axis: the destabilization of KSRP, which is responsible for the maintenance of oncosuppressive miRNAs.

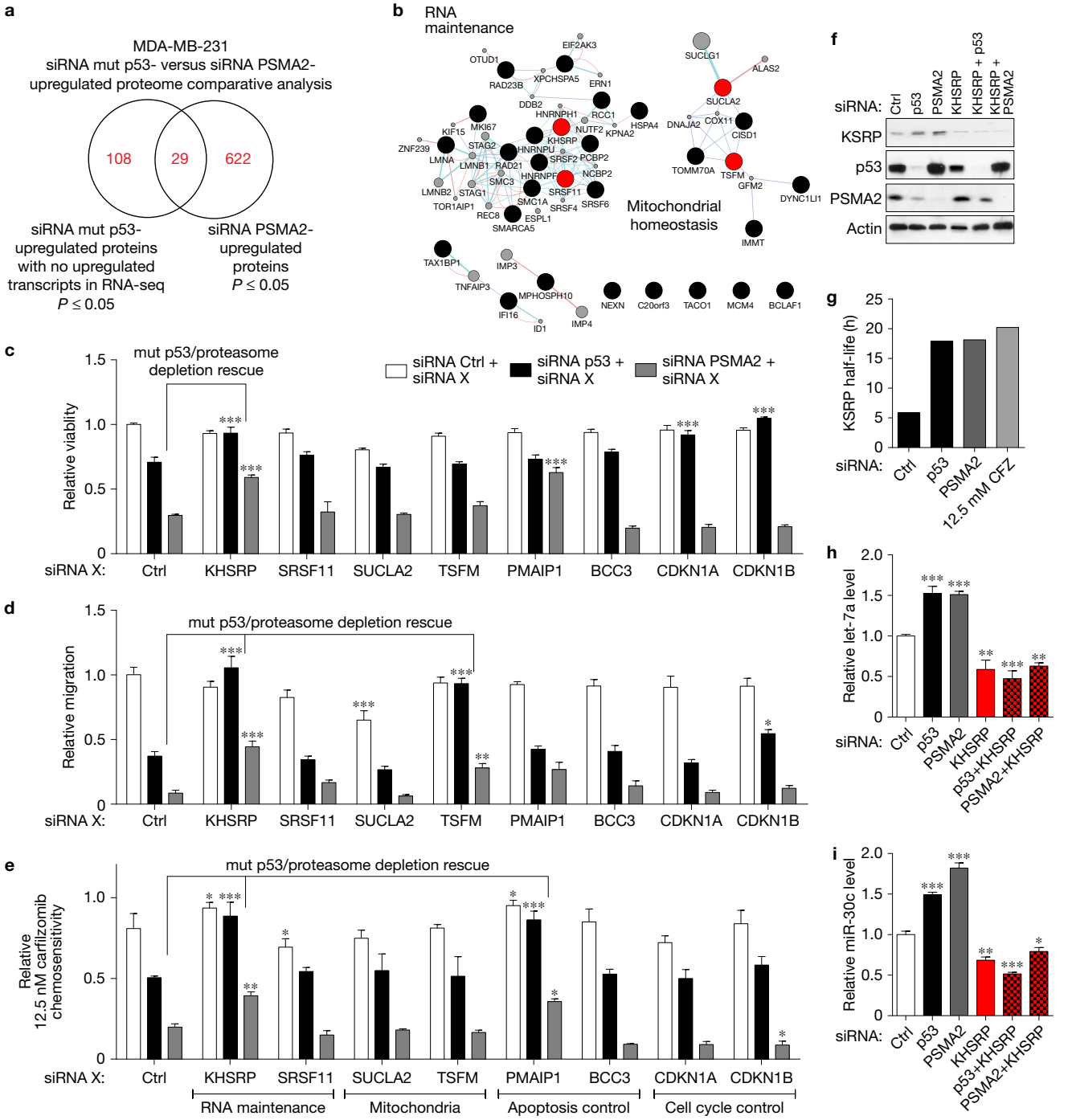

Figure 6 Mutant p53 exerts gain of function through the proteasome-mediated inhibition of tumour suppressors. (**a**) Venn diagram of proteins upregulated without matching changes in transcript levels on silencing of mutant *TP53* in MDA-MB-231 cells (see Fig. 1a) overlapped with proteins upregulated on silencing of the essential proteasome subunit gene *PSMA2* in MDA-MB-231 cells ($n = 4$ biologically independent samples for each silencing and condition, raw P value $P \leq 0.05$). (**b**) A GeneMania software-generated functional protein network of the 29 commonly upregulated proteins identified in **a** (dark blue lines—co-localization, light blue lines—common pathway involvement, light red lines—physical interactions). (**c**) Viability decrease induced by silencing of mutant *TP53* or of *PSMA2* suppressed by the concomitant silencing of the genes (siRNA X) encoding mutant p53 and proteasome-regulated factors in MDA-MB-231 cells. Significant suppression of the effect of silencing both *TP53* and *PSMA2* silencing is indicated. (**d**) As in **c** for the migration phenotype of MDA-MB-231 cells. (**e**) As in **c** for the carfilzomib chemoresistance phenotype of MDA-MB-231 cells. (**f**) KSRP protein level on mutant *TP53*/*PSMA2*/*KSRP* silencing in MDA-MB-231 cells (representative of three repeats). Unprocessed original scans of blots are shown in Supplementary Fig. 9. (**g**) KSRP protein half-life on silencing of mutant p53, *PSMA2* or carfilzomib (CFZ) treatment for 24 h in MDA-MB-231 cells. Full result is shown in Supplementary Fig. 5b. (**h**,**i**) Effects of *KSRP*/mutant *TP53*/*PSMA2* silencing on the levels of oncosuppressive miRNAs let-7a and miR-30c in MDA-MB-231 cells. **b**–**i** show means with s.d. of $n = 3$ biologically independent samples, ANOVA test with Bonferroni correction: $^{*}P < 0.05$, $^{**}P < 0.01$, $^{***}P < 0.001$. Additional results are shown in Supplementary Fig. 6. Statistics source data for **e**,**h**,**i** are provided in Supplementary Table 10.

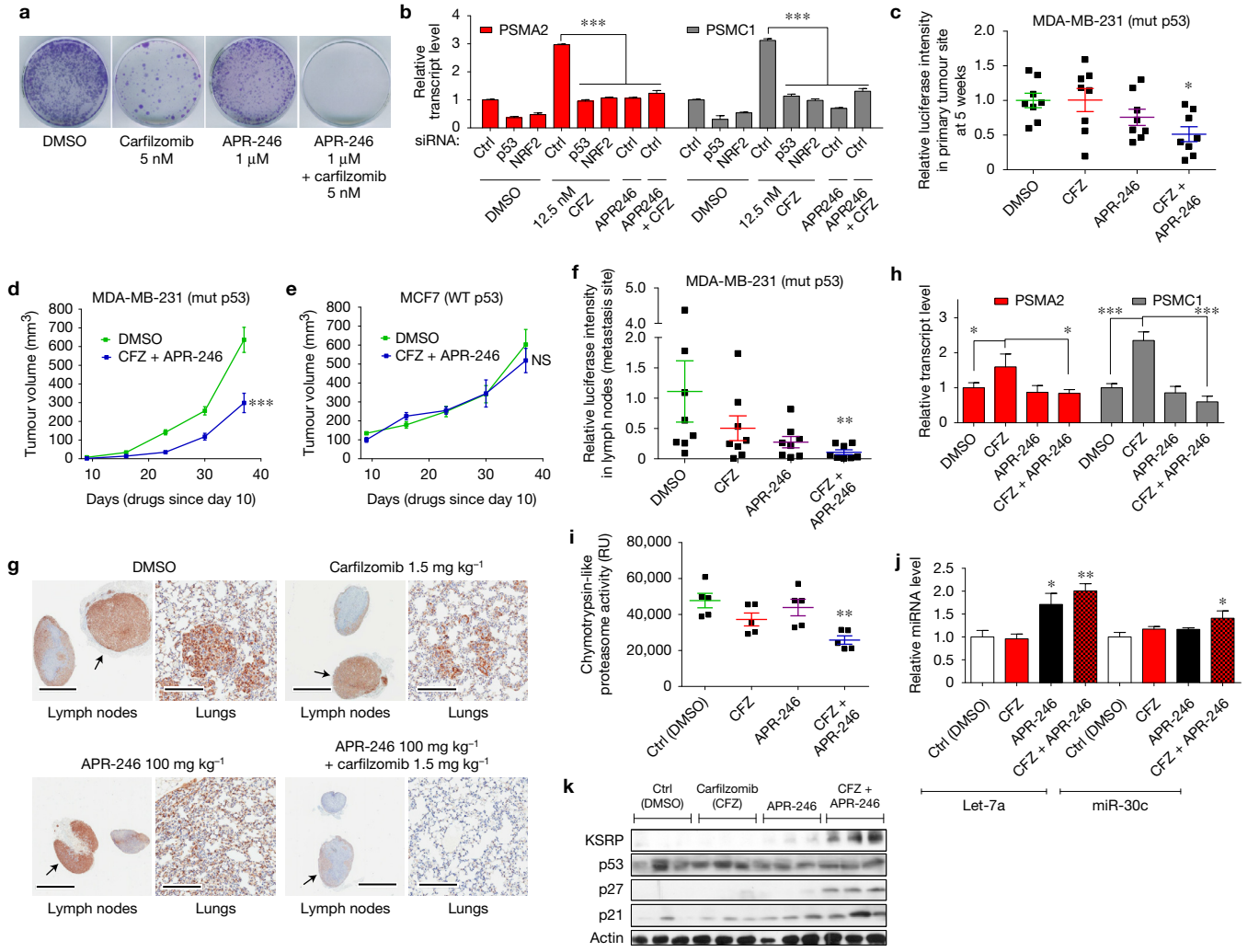

Figure 7 Mutant p53 targeting with APR-246 eliminates resistance to carfilzomib in TNBC cells. (**a**) Colony formation in the MDA-MB-231 cells under treatment with the indicated drugs (representative picture; see Supplementary Fig. 5e). (**b**) Effect of mutant *TP53*, *NRF2* silencing or APR-246 (PRIMA-1MET) on transcription of *PSMA2* and *PSMC1* genes, upregulated after treatment with carfilzomib (CFZ) in MDA-MB-231. (**c**) Luciferase *in vivo* intensity at primary tumour sites at 5 weeks of the MDA-MB-231–Luc mammary fat pad xenograft in SCID mice treated with DMSO, CFZ, APR-246 or a combination of CFZ and APR-246. (**d**) Primary MDA-MB-231–Luc xenograft growth in SCID mice treated with DMSO or a combination of CFZ and APR-246. (Calliper measurement means with s.e.m. for $n=8$ animals in each group, Friedman matched pairs test with Dunn's correction; $^{***}P<0.001$.) (**e**) MCF7 primary mammary fat pad xenograft growth in SCID mice treated as in **d**. (Calliper measurement means for $n=6$ animals in each group, test as in **d**—difference not significant (NS).) (**f**) Lymph-node area (metastasis) luciferase intensity in the mice from **c**,**d**. Data collected at 5 weeks for the DMSO group or later when treated tumours reached sizes comparable to controls. (**g**) Representative photos of lymph nodes (homolateral to the xenograft—indicated by arrows; bar size—2 mm) and lung tissue (bar size—200 μm) with immunohistochemical staining of the MDA-MB-231 metastasis (human cytokeratin, brown) in mice from **c**,**d**,**f**. See Supplementary Fig. 8. (**h**) *PSMA2* and *PSMC1* transcript levels in primary tumours extracted from mice in **c**,**d**. (**i**) Chymotrypsin-like proteasome activity in primary tumours, extracted as in **h**. (**j**) Levels of the miRNAs let-7a and miR-30c in primary tumours as in **h**. (**k**) KSRP, p53, p27, p21 and actin levels in primary tumours as in **h**. (Three representative lysates for each condition.) Unprocessed original scans of blots are shown in Supplementary Fig. 9. **b**,**c**,**f**,**h**–**j** show means with: s.d. for $n=3$ biologically independent samples for each condition (**b**) and with s.e.m. for $n=8$ animals (**c**,**f**) and $n=5$ animals (**h**–**j**). ANOVA test with Bonferroni correction; $^{*}P<0.05$, $^{**}P<0.01$, $^{***}P<0.001$. Additional results are shown in Supplementary Figs 7 and 8. Statistics source data for **b** are provided in Supplementary Table 10.

Targeting GOF p53 mutants with APR-246 (PRIMA-1MET) abrogates chemoresistance of TNBC cells to the proteasome inhibitor carfilzomib

The observation that the resistance of MDA-MB-231 cells to carfilzomib depends on mutant p53 (Fig. 6e) prompted us to investigate whether this effect could be significant in an *in vivo* tumour growth and metastasis model. Preliminarily we used in combination with carfilzomib, two clinically tested molecules known to inhibit the oncogenic activity of mutant p53—a histone deacetylase inhibitor SAHA (vorinostat) that downregulates the mutant p53 level[41] and PRIMA-1, which converts GOF p53 mutants into WT-like proteins[34,42] and abolishes the mutant p53–Nrf2 interaction (Fig. 5b).

The combination of carfilzomib and SAHA or PRIMA-1 acted synergistically to reduce cell viability and proteasome activity in the panel of five TNBC cell lines of interest, but not in MCF7 and MCF10A WT p53 cell lines (Supplementary Fig. 7a,b). However, in an *in vivo*

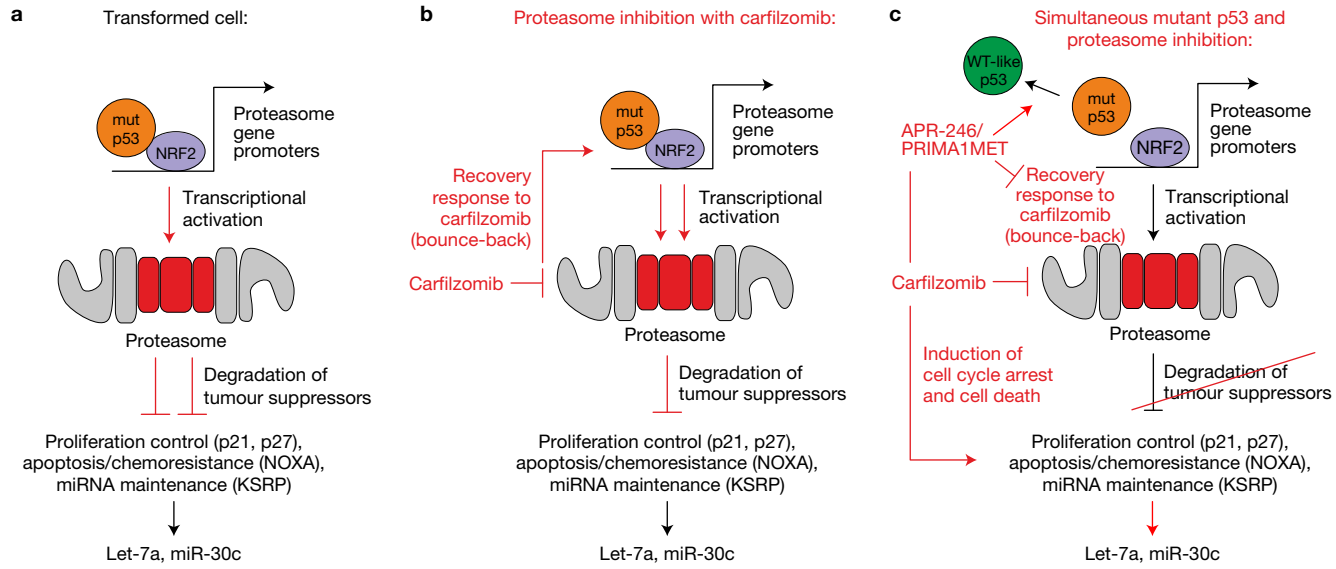

Figure 8 Model representation of mutant p53 regulation of the proteasome machinery and its therapeutic implication. (**a**) Mutant p53 activates proteasome gene transcription by controlling the Nrf2 transcription factor, which results in upregulation of proteasome activity and degradation of tumour suppressor proteins including KSRP—an oncosuppressive miRNA maturation factor. (**b**) Inhibition of the proteasome with carfilzomib results in the mutant p53- and Nrf2-mediated bounce-back response of the increased proteasome transcription. (**c**) Proteasome activity can be efficiently decreased by the simultaneous treatment of cells with carfilzomib and APR-246 (PRIMA-1MET)—a drug that converts mutant p53 to the wild-type-like form and reduces the interaction of mutant p53 with Nrf2.

MDA-MB-231 cell xenograft model[43], the combination with PRIMA-1 was more effective than with SAHA in reducing the primary tumour growth (Supplementary Fig. 7d). Thus, we introduced the PRIMA-1 phase I/II clinically tested derivative APR-246 (PRIMA-1MET) into further studies[44]. APR-246, just like PRIMA-1, showed an inhibitory effect on the proteasome activity and induced the WT p53 targets in MDA-MB-231 cells (Supplementary Fig. 7b,c). APR-246 was able to eradicate carfilzomib-resistant clones in colony-formation assays in MDA-MB-231 cells (Fig. 7a) in contrast to other chemotherapeutic drugs such as doxorubicin, cisplatin or paclitaxel (Supplementary Fig. 7e).

In response to proteasome inhibitors, cells engage a recovery 'bounce-back response' that upregulates proteasome gene transcription through the action of Nrf1 and Nrf2, leading to inhibitor resistance[45,46]. To evaluate this effect we treated the five TNBC cell lines with carfilzomib and observed a bounce-back increase of *PSMA2* and *PSMC1* gene expression that was abolished on *NRF2*, mutant *TP53* silencing or by the APR-246 treatment (Fig. 7b and Supplementary Fig. 7g).

In vivo, the combination of carfilzomib and APR-246 was more effective than single drug treatments in reducing the primary tumour growth of the mammary fat pad xenografts of MDA-MB-231 (Fig. 7c,d and Supplementary Fig. 7h), while the same drug combination had no effect on ER^+ primary tumours of WT p53 MCF7 xenografts (Fig. 7e). Importantly, the carfilzomib and APR-246 combination efficiently eradicated lymph-node and lung metastasis derived from the MDA-MB-231 xenograft (Fig. 7f,g and Supplementary Fig. 8).

Analysis of the MDA-MB-231 primary tumour biopsies indicated that the carfilzomib-induced 'bounce-back' of the proteasome was significantly blunted in mice treated with APR-246 (Fig. 7h,i), matching the *in vitro* results. Consistently, the levels of the tumour-suppressive miRNAs let-7a and miR30c increased most strongly in the xenografts treated with carfilzomib and APR-246 (Fig. 7j) and were accompanied by an increase in the levels of the KSRP protein and other tumour suppressors (Fig. 7k).

In summary, the combined drug-mediated inhibition of mutant p53 and the proteasome was able to block proliferation and metastatic dissemination of the TNBC cells *in vivo* (Fig. 8).

DISCUSSION

Here we provide evidence of a connection between two major tumour-promoting nodes in cancer—the GOF p53 mutants and the proteasome. Our findings highlight four aspects.

First, the proteasome machinery is a conserved representation of the mutant p53 transcriptional GOF. Previous studies reported regulation of proteasome subunits by mutant p53 without further investigation[47–50] or mutant p53-dependent activation of the proteasome activator REGγ (ref. 51). These studies, however, did not compare large-scale data from multiple models, and hence did not define which targets are shared between various p53 mutants and cell backgrounds. Our multi-omic and multi-model analyses led to identification of the proteasome subunit genes as the most over-represented common group of targets upregulated by multiple p53 missense mutant variants. Hence, at least the GOF p53 mutants that we have analysed can be regarded as a uniform oncogene—a notion supported by a recent study on shared properties of DNA interactomes of three mutant p53 variants[52].

Second, among the GOF effects the p53 mutants exert through formation of protein–protein complexes, the mutant p53 influence on the transcription factor Nrf2 may play a key role. Nrf2, whose pro- and antitumorigenic activities are both currently finding increasing experimental support[53], is a master regulator of the oxidative stress

response, known to cooperate with multiple oncogenes[54]. We show here that the proteasome genes controlled by Nrf2 and mutant p53 in normal conditions are also transactivated under oxidative stress, when stress response genes are repressed by mutant p53 (Supplementary Fig. 5g), as reported earlier[36]. This suggests that in cancer cells Nrf2 has two modes of regulation of its target promoters, possibly orchestrated by mutant p53: one towards the proteasome genes house-kept in cancer cells by Nrf2, and another towards the Nrf2-induced canonical oxidative stress response genes.

Third, our study broadens the understanding of known mutant p53 and proteasome negative impacts on the mechanisms of tumour suppression. The growth arrest reported in various experimental models following mutant *TP53* silencing[52,55,56] is shown here to depend not only on destabilization of known proteasome targets such as p21 and p27, but also on the proteasome-mediated destabilization of the KSRP protein, the mRNA splicing and miRNA maturation factor[37,57]. The effect on several phenotypic cancer manifestations observed on KSRP depletion can be explained by its role in the regulation of miRNAs, including let-7a and miR-30c, which possess tumour-suppressive activities related to cell growth, migration/invasion and chemoresistance[58,59]. The described mutant p53 and proteasome-mediated downregulation of let-7a and miR-30c extends the growing knowledge of miRNA targets of mutant p53[60–63].

Fourth, mutant p53, when present, is responsible for the resistance of TNBC cells to proteasome inhibitors. As the resistance to the proteasome inhibitors bortezomib and carfilzomib is a major issue in clinical practice, combinational therapies are being widely tested[64]. In our *in vitro* and *in vivo* experimental set-ups, combining carfilzomib with APR-246 effectively decreased the carfilzomib-induced bounce-back response of proteasome expression recovery. This treatment strategy may also overcome the limitations of therapies that target only mutant p53 in solid tumours, where combinational treatments have been avoided *in vivo*[2,65,66].

In summary, our study defines a common mutant p53 gain-of-function transcriptional program and links it to proteasome machinery activation. We explain how the transcriptional activity of mutant p53 and its effects on the protein degradation machinery co-shape the protein landscape of cancer cells. The simultaneous targeting of mutant p53 and the proteasome by APR-246 and carfilzomib (Fig. 8) provides a solution to overcome chemoresistance to proteasome inhibition in solid tumours and metastases harbouring mutant p53. □

ACKNOWLEDGEMENTS

We thank A. Testa for reading and editing the manuscript, and A. Kuczynski, L. Collavin, F. Mantovani, A. Rustighi and colleagues from LNCIB for helpful comments and discussions. We acknowledge K. Wiman and U. Björklund from Aprea for sharing the APR-246 compound and discussing the administration protocol. We thank D. D. Zhang for the gift of the Nrf2 expression vector. This work was supported by the European Research Council (ERC), the Italian Health Ministry and the Italian Association for Cancer Research (AIRC) to B.A. and the Italian Association for Cancer Research (AIRC) Special Program Molecular Clinical Oncology '5 per mille' (grant no. 10016) and the Italian Ministry of Health (RF-2011-02346976), to G.D.S.; Y.C. was supported by the AIRC/FIRC fellowship; K.G.-W. was supported by the Polish Academy of Sciences; D.W. was a recipient of the FEBS postdoctoral fellowship.

AUTHOR CONTRIBUTIONS

D.W. designed and performed the majority of the experiments, analysed the data, prepared the figures and wrote the paper. K.L. designed and performed the low-scale experiments, and prepared the figures. K.R., K.G.-W. and E.I. performed the low-scale experiments. R.S. and A.R. designed and performed the mouse xenograft experiments. S.P. and Y.C. performed the RNA-sequencing and the microarray data analysis and the patient data set association studies. C.T. and B.A. performed the ChIP-sequencing. M.J.M. and E.D. performed the ChIP-seq data analysis and the DNA motif identification. A.A., V.E. and A.Z. provided the human tumour samples, subtype identification, and p53 immunohistochemistry. J.R.W. performed the proteomic analysis and the proteomic data handling. G.D.S. supervised the project, designed experiments and wrote the paper.

COMPETING FINANCIAL INTERESTS

The authors declare no competing financial interests.

1. Kandoth, C. *et al.* Mutational landscape and significance across 12 major cancer types. *Nature* **502,** 333–339 (2013).
2. Walerych, D., Lisek, K. & Del Sal, G. Mutant p53: one, no one, and one hundred thousand. *Front. Oncol.* **5,** 289 (2015).
3. Di Agostino, S. *et al.* Gain of function of mutant p53: the mutant p53/NF-Y protein complex reveals an aberrant transcriptional mechanism of cell cycle regulation. *Cancer Cell* **10,** 191–202 (2006).
4. Song, H., Hollstein, M. & Xu, Y. p53 gain-of-function cancer mutants induce genetic instability by inactivating ATM. *Nat. Cell Biol.* **9,** 573–580 (2007).
5. Muller, P. A. *et al.* Mutant p53 drives invasion by promoting integrin recycling. *Cell* **139,** 1327–1341 (2009).
6. Adorno, M. *et al.* A mutant-p53/Smad complex opposes p63 to empower TGFβ-induced metastasis. *Cell* **137,** 87–98 (2009).
7. Stambolsky, P. *et al.* Modulation of the vitamin D3 response by cancer-associated mutant p53. *Cancer Cell* **17,** 273–285 (2010).
8. Girardini, J. E. *et al.* A Pin1/mutant p53 axis promotes aggressiveness in breast cancer. *Cancer Cell* **20,** 79–91 (2011).
9. Freed-Pastor, W. A. *et al.* Mutant p53 disrupts mammary tissue architecture via the mevalonate pathway. *Cell* **148,** 244–258 (2012).
10. Freed-Pastor, W. A. & Prives, C. Mutant p53: one name, many proteins. *Genes Dev.* **26,** 1268–1286 (2012).
11. Walerych, D., Napoli, M., Collavin, L. & Del Sal, G. The rebel angel: mutant p53 as the driving oncogene in breast cancer. *Carcinogenesis* **33,** 2007–2017 (2012).
12. Shah, S. P. *et al.* The clonal and mutational evolution spectrum of primary triple-negative breast cancers. *Nature* **486,** 395–399 (2012).
13. Turner, N. *et al.* Targeting triple negative breast cancer: is p53 the answer? *Cancer Treat. Rev.* **39,** 541–550 (2013).
14. Eldridge, A. G. & O'Brien, T. Therapeutic strategies within the ubiquitin proteasome system. *Cell. Death Differ.* **17,** 4–13 (2010).
15. Ben-Nissan, G. & Sharon, M. Regulating the 20S proteasome ubiquitin-independent degradation pathway. *Biomolecules* **4,** 862–884 (2014).
16. Wang, M. Comparative mechanisms of action of proteasome inhibitors. *Oncology (Williston Park)* **25,** 19–24 (2011).
17. Nijhawan, D. *et al.* Cancer vulnerabilities unveiled by genomic loss. *Cell* **150,** 842–854 (2012).
18. Petrocca, F. *et al.* A genome-wide siRNA screen identifies proteasome addiction as a vulnerability of basal-like triple-negative breast cancer cells. *Cancer Cell* **24,** 182–196 (2013).
19. Johnson, D. E. The ubiquitin-proteasome system: opportunities for therapeutic intervention in solid tumors. *Endocr. Relat. Cancer* **22,** T1-17 (2015).
20. Wisniewski, J. R. & Mann, M. Consecutive proteolytic digestion in an enzyme reactor increases depth of proteomic and phosphoproteomic analysis. *Anal. Chem.* **84,** 2631–2637 (2012).
21. Wisniewski, J. R. & Rakus, D. Multi-enzyme digestion FASP and the 'Total Protein Approach'-based absolute quantification of the *Escherichia coli* proteome. *J. Proteom.* **109,** 322–331 (2014).
22. Cho, Y., Gorina, S., Jeffrey, P. D. & Pavletich, N. P. Crystal structure of a p53 tumor suppressor-DNA complex: understanding tumorigenic mutations. *Science* **265,** 346–355 (1994).
23. Allen, M. A. *et al.* Global analysis of p53-regulated transcription identifies its direct targets and unexpected regulatory mechanisms. *Elife* **3,** e02200 (2014).
24. Tonelli, C. *et al.* Genome-wide analysis of p53 transcriptional programs in B cells on exposure to genotoxic stress *in vivo*. *Oncotarget* **6,** 24611–24626 (2015).
25. Younger, S. T., Kenzelmann-Broz, D., Jung, H., Attardi, L. D. & Rinn, J. L. Integrative genomic analysis reveals widespread enhancer regulation by p53 in response to DNA damage. *Nucleic Acids Res.* **43,** 4447–4462 (2015).

26. Janky, R. *et al.* iRegulon: from a gene list to a gene regulatory network using large motif and track collections. *PLoS Comput. Biol.* **10,** e1003731 (2014).
27. Lang, G. A. *et al.* Gain of function of a p53 hot spot mutation in a mouse model of Li-Fraumeni syndrome. *Cell* **119,** 861–872 (2004).
28. Steffen, J., Seeger, M., Koch, A. & Kruger, E. Proteasomal degradation is transcriptionally controlled by TCF11 via an ERAD-dependent feedback loop. *Mol. Cell* **40,** 147–158 (2010).
29. Vangala, J. R., Dudem, S., Jain, N. & Kalivendi, S. V. Regulation of PSMB5 protein and β subunits of mammalian proteasome by constitutively activated signal transducer and activator of transcription 3 (STAT3): potential role in bortezomib-mediated anticancer therapy. *J. Biol. Chem.* **289,** 12612–12622 (2014).
30. Moschonas, A. *et al.* CD40 induces antigen transporter and immunoproteasome gene expression in carcinomas via the coordinated action of NF-κB and of NF-κB-mediated *de novo* synthesis of IRF-1. *Mol. Cell Biol.* **28,** 6208–6222 (2008).
31. Xu, H. *et al.* The CCAAT box-binding transcription factor NF-Y regulates basal expression of human proteasome genes. *Biochim. Biophys. Acta* **1823,** 818–825 (2012).
32. Weisz, L. *et al.* Mutant p53 enhances nuclear factor κB activation by tumor necrosis factor α in cancer cells. *Cancer Res.* **67,** 2396–2401 (2007).
33. Drost, J. *et al.* BRD7 is a candidate tumour suppressor gene required for p53 function. *Nat. Cell Biol.* **12,** 380–389 (2010).
34. Lambert, J. M. *et al.* PRIMA-1 reactivates mutant p53 by covalent binding to the core domain. *Cancer Cell* **15,** 376–388 (2009).
35. Chen, W. *et al.* Direct interaction between Nrf2 and p21(Cip1/WAF1) upregulates the Nrf2-mediated antioxidant response. *Mol. Cell* **34,** 663–673 (2009).
36. Kalo, E. *et al.* Mutant p53R273H attenuates the expression of phase 2 detoxifying enzymes and promotes the survival of cells with high levels of reactive oxygen species. *J. Cell. Sci.* **125,** 5578–5586 (2012).
37. Trabucchi, M. *et al.* The RNA-binding protein KSRP promotes the biogenesis of a subset of microRNAs. *Nature* **459,** 1010–1014 (2009).
38. Listerman, I., Sun, J., Gazzaniga, F. S., Lukas, J. L. & Blackburn, E. H. The major reverse transcriptase-incompetent splice variant of the human telomerase protein inhibits telomerase activity but protects from apoptosis. *Cancer Res.* **73,** 2817–2828 (2013).
39. Desideri, E., Vegliante, R. & Ciriolo, M. R. Mitochondrial dysfunctions in cancer: genetic defects and oncogenic signaling impinging on TCA cycle activity. *Cancer Lett.* **356,** 217–223 (2015).
40. Boland, M. L., Chourasia, A. H. & Macleod, K. F. Mitochondrial dysfunction in cancer. *Front. Oncol.* **3,** 292 (2013).
41. Li, D., Marchenko, N. D. & Moll, U. M. SAHA shows preferential cytotoxicity in mutant p53 cancer cells by destabilizing mutant p53 through inhibition of the HDAC6-Hsp90 chaperone axis. *Cell. Death Differ.* **18,** 1904–1913 (2011).
42. Wiman, K. G. Pharmacological reactivation of mutant p53: from protein structure to the cancer patient. *Oncogene* **29,** 4245–4252 (2010).
43. Rustighi, A. *et al.* The prolyl-isomerase Pin1 is a Notch1 target that enhances Notch1 activation in cancer. *Nat. Cell Biol.* **11,** 133–142 (2009).
44. Lehmann, S. *et al.* Targeting p53 *in vivo*: a first-in-human study with p53-targeting compound APR-246 in refractory hematologic malignancies and prostate cancer. *J. Clin. Oncol.* **30,** 3633–3639 (2012).
45. Radhakrishnan, S. K. *et al.* Transcription factor Nrf1 mediates the proteasome recovery pathway after proteasome inhibition in mammalian cells. *Mol. Cell* **38,** 17–28 (2010).
46. Arlt, A. *et al.* Inhibition of the Nrf2 transcription factor by the alkaloid trigonelline renders pancreatic cancer cells more susceptible to apoptosis through decreased proteasomal gene expression and proteasome activity. *Oncogene* **32,** 4825–4835 (2013).
47. Weissmueller, S. *et al.* Mutant p53 drives pancreatic cancer metastasis through cell-autonomous PDGF receptor β signaling. *Cell* **157,** 382–394 (2014).
48. Polotskaia, A. *et al.* Proteome-wide analysis of mutant p53 targets in breast cancer identifies new levels of gain-of-function that influence PARP, PCNA, and MCM4. *Proc. Natl Acad. Sci. USA* **112,** E1220–E1229 (2015).
49. Do, P. M. *et al.* Mutant p53 cooperates with ETS2 to promote etoposide resistance. *Genes Dev.* **26,** 830–845 (2012).
50. Martynova, E. *et al.* Gain-of-function p53 mutants have widespread genomic locations partially overlapping with p63. *Oncotarget* **3,** 132–143 (2012).
51. Ali, A. *et al.* Differential regulation of the REGγ-proteasome pathway by p53/TGF-β signalling and mutant p53 in cancer cells. *Nat. Commun.* **4,** 2667 (2013).
52. Zhu, J. *et al.* Gain-of-function p53 mutants co-opt chromatin pathways to drive cancer growth. *Nature* **525,** 206–211 (2015).
53. Jaramillo, M. C. & Zhang, D. D. The emerging role of the Nrf2-Keap1 signaling pathway in cancer. *Genes Dev.* **27,** 2179–2191 (2013).
54. DeNicola, G. M. *et al.* Oncogene-induced Nrf2 transcription promotes ROS detoxification and tumorigenesis. *Nature* **475,** 106–109 (2011).
55. Di Minin, G. *et al.* Mutant p53 reprograms TNF signaling in cancer cells through interaction with the tumor suppressor DAB2IP. *Mol. Cell* **56,** 617–629 (2014).
56. Kollareddy, M. *et al.* Regulation of nucleotide metabolism by mutant p53 contributes to its gain-of-function activities. *Nat. Commun.* **6,** 7389 (2015).
57. Bikkavilli, R. K. & Malbon, C. C. Dishevelled-KSRP complex regulates Wnt signaling through post-transcriptional stabilization of β-catenin mRNA. *J. Cell. Sci.* **123,** 1352–1362 (2010).
58. Liu, K. *et al.* Let-7a inhibits growth and migration of breast cancer cells by targeting HMGA1. *Int. J. Oncol.* **46,** 2526–2534 (2015).
59. Hummel, R., Hussey, D. J. & Haier, J. MicroRNAs: predictors and modifiers of chemo- and radiotherapy in different tumour types. *Eur. J. Cancer* **46,** 298–311 (2010).
60. Garibaldi, F. *et al.* Mutant p53 inhibits miRNA biogenesis by interfering with the microprocessor complex. *Oncogene* http://dx.doi.org/10.1038/onc.2016.51 (2016).
61. Subramanian, M. *et al.* A mutant p53/let-7i-axis-regulated gene network drives cell migration, invasion and metastasis. *Oncogene* **34,** 1094–1104 (2015).
62. Masciarelli, S. *et al.* Gain-of-function mutant p53 downregulates miR-223 contributing to chemoresistance of cultured tumor cells. *Oncogene* **33,** 1601–1608 (2014).
63. Neilsen, P. M. *et al.* Mutant p53 drives invasion in breast tumors through up-regulation of miR-155. *Oncogene* **32,** 2992–3000 (2013).
64. Huang, Z. *et al.* Efficacy of therapy with bortezomib in solid tumors: a review based on 32 clinical trials. *Future Oncol.* **10,** 1795–1807 (2014).
65. Bykov, V. J. & Wiman, K. G. Mutant p53 reactivation by small molecules makes its way to the clinic. *FEBS Lett.* **588,** 2622–2627 (2014).
66. Girardini, J. E., Marotta, C. & Del Sal, G. Disarming mutant p53 oncogenic function. *Pharmacol. Res.* **79,** 75–87 (2014).

METHODS

Cell lines. The human cell lines MDA-MB-231 (p53 R280K), MDA-MB-468 (p53 R273H), HCC-1395 (p53 R175H), PANC-1 (p53 R273H), HT-29 (p53 R273H) and 293GP (p53 WT) and mouse embryonic fibroblasts (MEF—for p53 status see below) were cultured in DMEM medium (Sigma) with 10% FCS (Euroclone), and antibiotics (Lonza).

BT-549 (p53 R249S), DU145 (heterozygous p53—P223L/V274F), H1299 (p53-null) and TOV112 (p53 R175H) cells were cultured in RPMI medium (Sigma) supplemented with 10% FBS and antibiotics.

SUM-149 (p53 M237I) cells were cultured in DMEM/F12 Ham's medium 1:1, supplemented with 10% FCS and antibiotics.

MCF7 (p53 WT) were cultured in EMEM (Sigma), supplemented with 1% non-essential amino acid solution (Sigma), 10% FBS and antibiotics. Mahlavu cells (p53 R249S) were grown as MCF7, with addition of 2 mM L-glutamine.

MCF10A (p53 WT, shRNA p53 and stable mutant p53-overexpressing cell lines) cells were maintained in DMEM/F12 Ham's medium 1:1, supplemented with 5% horse serum, insulin (10 $\mu g\,ml^{-1}$), hydrocortisone (0.5 $\mu g\,ml^{-1}$) and epidermal growth factor (EGF 20 $ng\,ml^{-1}$), if needed—with addition of selection antibiotics.

Mutant p53 cell lines have been confirmed to express the indicated mutant *TP53* variants by sequencing of the full-length p53 mRNA.

MEFs were generated by crossing mice of the appropriate genotype, and collecting cells from 13.5 d.p.c. embryos. MEF KO p53 and MEF KI p53R172H were optionally immortalized through retroviral transduction of H-Ras V12 as described previously[8].

All of the cell lines have been tested by PCR/IF for *Mycoplasma* presence.

All human cell lines were authenticated by using STR genotyping with the PowerPlex 18D System and confirmed in their identity by comparing the results to reference cell databases (DMSZ, ATCC, and JCRB databases).

No cell lines used in this study were found in the database of commonly misidentified cell lines that is maintained by ICLAC and NCBI Biosample.

Plasmids. pSR–shRNAp53 PuroR was a gift from R. Agami (The Netherlands Cancer Institute, The Netherlands). N-terminally HA-tagged p53 constructs were generated by first introducing 4 silent point mutations in the region targeted by p53 siRNA I/shRNA by site-directed mutagenesis in pcDNA-HA-p53, subsequent introduction of missense point mutations and subcloning of sequenced p53 cds constructs to the pMSCV–HA BlastR retroviral vector.

Transfection. For retrovirus production, low-confluence HEK 293GP packaging cells were transfected with appropriate vectors by calcium phosphate. After 48–72 h the virus-containing medium was filtered and added to target cells (MDA-MB-231 or MCF10A). Cells were selected with puromycin (0.5 $\mu g\,ml^{-1}$) and/or blasticidin (2 $\mu g\,ml^{-1}$).

H1299 cells were transfected using Lipofectamine 2000 (Invitrogen) as in the manufacturer's instructions. For siRNA transfections, all cells lines were transfected 2× using Lipofectamine RNAiMax (Invitrogen). After 48 h of the second silencing, cells were processed.

siRNA sequences are listed in Supplementary Table 7.

Total RNA extraction and RT–qPCR of mRNA and miRNA. Total RNA was extracted with QIAzol (Qiagen) following the manufacturer's instructions. One microgram of total RNA was reverse-transcribed with QuantiTect Reverse Transcription (Qiagen). qPCR was performed using SsoAdvancedTMSYBR Green Master Mix (Bio-Rad) on a CFX96 Real-Time PCR System (Bio-Rad). miRNAs were retrotranscribed using the miScript kit (Qiagen) and qPCR was performed using QuantiTect SYBR Green Master Mix (Qiagen) and primer kits (MS00031220, MS00009366; Qiagen). The list of qPCR primers is provided in Supplementary Table 7.

RNA-seq and low-level analysis. MDA-MB-231 mRNA-seq libraries were obtained by the Illumina TruSeq library construction kit using total RNA from the cell line transfected with control siRNA or p53 siRNA I. mRNA-seq libraries were sequenced using Illumina HiSeq2000 for 100 bp paired-end sequencing. Quality control of mRNA-seq data was performed using Fatsqc (www.bioinformatics.babraham.ac.uk/projects/fastqc). Read files were mapped to the human genome (hg19) and analysed for differential expression using the Tuxedo software suite implemented in the Galaxy workflow manager. The mapping was performed by Tophat2 and Cufflinks was used to find out differential expressed genes. *P* values are adjusted for multiple testing using the Benjamini–Hochberg correction.

Microarray hybridization and low-level analysis. For gene expression profiling in the MDA-MB-468, BT-549, SUM-149PT and HCC1395 cell lines, we used the Illumina HumanHT-12-v4-BeadChip (Illumina). Total RNA isolated from the used cell lines expressing control siRNA and p53 siRNA I was reverse transcribed and amplified. cRNA was hybridized onto each array and then labelled with Cy3–streptavidin (Amersham Biosciences). The array was scanned using a BeadStation 500 system (Illumina). The probe intensities were calculated and normalized using GenomeStudio Data Analysis Software's Gene Expression Module (GSGX) Version 1.9 (Illumina). Further data processing was performed in the R computing environment version 3.0 (http://www.r-project.org), with BioConductor packages (http://www.bioconductor.org). Statistical analysis for differentially expressed genes was performed with limma. *P* values were adjusted for multiple testing using Benjamini and Hochberg's method. To generate annotated expression matrices for cluster analysis, mapped reads were counted with HTSeq (v0.6, http://www-huber.embl.de/users/anders/HTSeq). The counts were normalized for the library sizes using the calcNormFactors in edgeR citation.

Cluster and principal component analysis. Starting from the annotated expression matrices, after *Z*-score standardization, features with low standard deviation were filtered out. To obtain a comparable number of genes between the two platforms (RNA-seq and Illumina microarrays) for the cluster analysis, we set the standard deviation threshold as 0.1 for microarrays data and as 0.05 for RNA-seq data. Unsupervised hierarchical cluster analysis was performed using Cluster software (EisenLab). Cluster results were then visualized using Java TreeView.

Principal component analysis was performed on the five-cell-line expression matrix considering only the common genes between RNA-seq and Illumina microarrays (genes = 16,994), using all of the samples ($n = 30$). We used the R/Bioconductor Environment both for calculation and plotting the results.

Feature selection. To extract a smaller subset of the whole proteasome 37-gene signature with a greater correlation to poor prognosis first we performed a feature selection analysis to select the most informative proteasome genes in respect to the *TP53* status. The recursive feature selection incorporating resampling, in particular the leave-one-out cross-validation (LOOCV with repeat = 100, number = 100) method, was implemented in the Caret package in the R/Biocondictor environment[67].

ChIP and ChIP-sequencing. ChIP was performed essentially as described previously[8] with modification of the cell lysis and sonication stage to produce DNA fragments suitable for ChIP-sequencing: cells were lysed in lysis buffer—50 mM HEPES pH 7.9, 140 mM NaCl, 1 mM EDTA, 10% glycerol, 0.5% NP-40, 0.25% Triton X-100, nuclei spun down, washed in 10 mM Tris-HCl, pH 7.5, 200 mM NaCl, 1 mM EDTA and resuspended in shearing buffer—0.1% SDS, 1 mM EDTA, 10 mM Tris, pH 7.5. Samples were sonicated using a Bioruptor sonicator (Diagenode; medium power setting) for the total time of 30 min, to achieve an average size of 250–300 bp of the sonicated chromatin fragments. The shearing buffer was then supplemented to obtain the RIPA buffer of the composition described in ref. 8 and the rest of the protocol was followed. For the used mouse (anti- p53, p300) and rabbit (anti-Nrf1, Nrf2, acetyl-H3K9, histone H3) ChIP antibodies the species-matched IgG nonspecific antibodies were used as controls.

For the ChIP-sequencing, 2–10 ng DNA resulting from the ChIP procedure described above, obtained from six 15 cm plates of MDA-MB-231 per IP, was prepared for HiSeq2000 sequencing with the TruSeq ChIP Sample Prep Kit (Illumina) following the manufacturer's instructions.

ChIP-seq peak calling and artefact filtering. ChIP-seq NGS reads were aligned to the hg19 genome through the BWA aligner using default settings.

We identified significant peaks using the Model-based Analysis of ChIP-Seq (MACS, version 1.0.1) program, integrated in the Galaxy platform. We considered the reads as reliable mutant p53-binding sites if the *P* value was $\leq 1.00 \times 10^{-5}$ and fold enrichment (FE) ≥ 10. FDR is calculated as described in the MACS manual. We used the Genomic Regions Enrichment of Annotations Tool (GREAT, version 2.0.2) to associate MACS peaks to nearby genes within a distance of ± 500 bp from peaks to gene TSS.

Enriched transcription factor binding sites discovery. We selected the ChIP-seq peaks of 37 human proteasome genes and obtained the nucleotide sequences corresponding to the genomic regions ± 150 bp. We identified enriched transcription factor binding sites using the LASAGNA-Search web tool (version 2.0). We adjusted *P* values for multiple testing using the Benjamini–Hochberg's method, retaining only sites with counts ≥ 20.

For all sites with maximum similarity, we created consensus sequences using WebLogo (version 3.4). Finally, we re-aligned every consensus sequence to its original predicted transcription factor binding site using the TOMTOM Motif Comparison Tool (version 4.9.1, integrated in the MEME suite), keeping only the sites with a *P* value $< 1.00 \times 10^{-4}$ (Pearson correlation coefficient) with respect to binding sites of the 'Vertebrates (*In vivo* and *in silico*)' database.

Proteomic analysis. MDA-MB-231 cells transfected with control siRNA, p53 siRNA I or PSMA2 siRNA were lysed in 50 mM Tris-HCl, pH 7.8 containing 2% (w/v) SDS and 0.1 M dithiothreitol and the lysates were processed by the MED FASP procedure with consecutive protein cleavages using LysC and trypsin[20]. The released peptides were loaded on strong anion exchange microcolumns and were eluted with Britton–Robinson universal buffer at pH 5 and pH 2. The fractions were analysed by LC–MS/MS using an LTQ-Orbitrap instrument as described previously[20]. Spectra were searched by MaxQuant software (www.maxquant.org) and the concentrations of proteins were assessed by the total protein approach using the raw protein intensities[21]. *t*-test was used to assess *P* value support of differences between protein concentrations in distinct experimental conditions.

Gene signatures, functional annotation and pathway enrichment analysis. Full transcriptomic, proteomic or ChIP-seq expression data sets have been imported to Ingenuity Pathway Analysis (IPA) software (Qiagen, www.ingenuity.com). *P* value and log fold-change cutoffs were applied in IPA as described in the text and figures. IPA was used to overlap data sets, to generate data for Venn diagrams and produce resulting signature gene/protein lists.

The pathway analysis module of IPA was used to associate analysed signatures with molecular pathways.

An independent, parallel method for analysing the signatures was the pathway-related gene ontology term enrichment analysis, using the ClueGO plugin[68] for the Cytoscape environment (http://www.cytoscape.org).

For proteomic data functional analysis the GeneMania plugin for Cytoscape[69] was used, allowing us to analyse cellular co-localization, interaction and pathway association simultaneously (otherwise default settings were employed).

Statistics and reproducibility. The statistical analysis of the experimental results is described in the figure legends, along with the number of samples analysed and the plotted error types (s.d.—standard deviation; s.e.m.—standard error of the mean). Statistic tests were performed and *P* value thresholds were obtained using GraphPad 6.0. In cases where data from averages of two experiments are shown, raw data are provided in Supplementary Table 10. Western blots and IF experiments were performed in at least two replicates; the representative is shown. Additional details are given in appropriate Methods sections. See the Data availability section for statistics source data distribution in the Supplementary Tables. No statistical method was used to predetermine sample sizes. Mice in mouse xenograft experiments were randomized both before cell injection and before treatment. The investigators were blinded to sample allocation only in proteasome activity measurements in human tumour samples (Fig. 3b).

Patient survival and mutation status association analysis. To verify the correlation of the gene signatures and breast cancer clinical data, survival analysis was performed on a breast cancer meta-data set composed by 3,458 samples using the Km-plotter online analysis tool. To perform the analysis on the greatest possible number of patients, for each gene, we selected only HGU133A probe sets. The samples were split into two groups according to quantile expressions of the proposed signatures. The two groups were then compared by survival analysis. The Kaplan–Maier curves of relapse-free survival time, the hazard ratio with 95% confidence intervals and log-rank test *P* values were calculated. As we are investigating the effect of mutant p53 in cancer patients we inverted the signs of expression fold change coming from the mutant *TP53* silencing experiments. For each signature we selected the top 30 upregulated and the top 30 downregulated genes; the 37-gene whole proteasome signature was fully analysed (Km-plotter online tool permits one to combine up to 65 genes). To combine upregulated and downregulated genes in the same analysis, to the genes that are downregulated in the signatures (upregulated after silencing of mutant *TP53*) a negative weight has been assigned, so the less they are expressed, the more the signature is considered highly expressed.

Gene expression data, *TP53* mutation status and clinical annotation for different cancer types (TCGA data sets) were obtained from the Cancer Genomics Data Server using the cgdsr package for R. The data sets were chosen for analysis according to the WT *TP53* versus mutant *TP53* status availability, with *TP53*-null samples excluded. For each patient we defined the levels of a 37-gene signature expression as the mean of the expression values of all the genes included in the signature. The statistical differences between the distributions of expression values in the two molecular conditions (mutated *TP53* and WT *TP53*) were calculated by Mann–Whitney *U*-test in the R/Bioconductor environment.

Pearson's chi-squared test with Yates' continuity correction was performed to test independence between TP53 status and a signature expression.

Western blot analysis. Total cell extracts were prepared in RIPA buffer without SDS (150 mM NaCl, 50 mM Tris-HCl pH 8, 1 mM EDTA, 1% NP-40, 0.5% Na deoxycholate) supplemented with 1 mM phenylmethylsulfonyl fluoride, 5 mM NaF, 1 mM Na_3VO_4, 10 μg ml^{-1} CLAP protease inhibitor cocktail (SIGMA). Protein concentration was determined with Bio-Rad Protein Assay Reagent (Bio-Rad). Lysates were resolved by SDS–PAGE and transferred to nitrocellulose (Millipore). Western blot analysis was performed according to standard procedures. The antibodies used are listed in Supplementary Table 11.

Protein stability determination. Cells treated for 24 h with DMSO or carfilzomib or 48 h post indicated siRNA transfection were treated with 0.1 mg ml^{-1} cycloheximide (CHX; Sigma) and lysed in SDS–PAGE loading buffer directly on plates at the indicated time points. Lysates were subjected to western blots and the results were scanned and analysed densitometrically by ImageJ. The results were plotted in Excel and protein half-lives were determined according to the fitted exponential decay equations.

Proteasome activity assay. Adherent cells were washed with PBS, scraped from plates and lysed at 4 °C in a lysis buffer containing 1% NP-40, 1% deoxycholate, 100 mM NaCl at pH 7.5, and the remains were spun down. In the case of tissue (tumour) samples, homogenization was used in the lysis buffer followed by centrifugation to remove solid remains. Fifty micrograms of total protein was used per one measurement. Even volumes of the protein extracts were resuspended in 1× assay buffer (20S Proteasome Activity Assay Kit, Chemicon-Millipore) containing 25 mM HEPES pH 7.5, 0.5 mM EDTA, 0.05% NP-40, 0.001% SDS to the volume of 90 μl per measurement and supplemented with 10 μl of 0.5 mM proteasome substrates (Millipore): Substrate III (Suc-LLVY-AMC, chymotrypsin-like activity), Substrate IV (Z-ARR-AMC, trypsin-like activity). Samples with substrates in 96-well black plates were incubated at 37 °C for 2 h and measured using an EnSpire plate fluorometer (Perkin Elmer). Controls, sensitivity calibration and standard curves were made on the basis of recommendations of the 20S Proteasome Activity Assay Kit (Chemicon-Millipore).

Protein interaction studies. Co-immunoprecipitation experiments of endogenous proteins were performed by lysing cells in the Co-IP buffer (NaCl 150 mM, Tris-HCl pH 8 50 mM, EDTA 1 mM, NP-40 0.5%, glycerol 10%) with protease inhibitors. Samples were cleared by centrifugation for 30 min at 13,000*g* at 4 °C and incubated overnight at 4 °C with the specific antibody. After 1 h incubation with protein G–Sepharose (GE Healthcare), immunoprecipitates were washed three times in Co-IP buffer, resuspended in a sample buffer, and analysed by western blotting. For Co-IP of endogenous p53 or Nrf2, DO-1 (sc-126, Santa Cruz) and EP1808Y (ab62352, Abcam) primary antibodies were used respectively.

The GST pulldown assay was performed essentially as described earlier[70]. Nrf2 was detected using anti-Nrf2 antibody and overexpressed GST-fusion proteins were detected by Ponceau-Red staining of the western blot membrane.

Immunofluorescence. IF was performed as described previously[55] using primary antibodies against p53 and Nrf2: DO-1 (sc-126, Santa Cruz) and EP1808Y (ab62352, Abcam).

Cell fractionation. To evaluate Nrf2 and p53 cellular localization, nuclear and cytosolic fractions were prepared using the ProteoExtract Subcellular Proteome Extraction Kit (Millipore), following the manufacturer's instructions. Proteins were detected on western blots using the indicated antibodies.

Cell cycle FACS analysis and migration assay. These analyses were performed as described earlier[55].

Viability assay. Cells (6–10 × 10^4) were plated in 96-well plates (white, transparent bottom), and after 24 h they were treated as indicated in the figures and assayed for viability post 24 h using ATPlite OneStep reagent (Perkin Elmer), according to the manufacturer's instructions.

Colony-formation assay. Four thousand cells were plated on 6 cm plates in serum-containing medium. After 48 h, the medium was supplemented with drugs as indicated in the figures. The medium and drugs were replaced every 3 days. After 12–14 days with drugs, the cells were fixed (formaldehyde 37%, diluted 1:10 in PBS) and stained for 15 min with Giemsa diluted solution 1:10 in water (Fluka). Plates washed with water and dried were analysed microscopically.

Human breast cancer specimens. Human breast cancer tissues for research purposes were provided by the institutional biobank at IRCCS Fondazione Salvatore Maugeri (FSM). This study was approved by the FSM Central Ethic Committee and subject to patients' informed consent. Tumour samples were selected on the basis of histopathological analysis performed by the Unit of Pathology at FSM. Frozen tumour tissue was fragmented by mortar and pestle in liquid nitrogen, and fragments were split 1:1 into Quiazol (see Total RNA extraction) and lysis buffer (see Proteasome activity assay) and homogenized mechanically. Samples were further

processed according to RNA extraction and proteasome activity assay protocols. For p53 cds mRNA sequencing the cDNA produced from total mRNA was used as a template for PCR of full-length p53 cds and the product was sequenced.

Immunohistochemistry. For p53 staining in breast cancer tissues, FFPE slices from each cancer sample along with its normal counterpart (as control) were processed. Epitope retrieval was performed in pre-warmed TE buffer, pH 9 for 40 min at 98 °C. For antigen detection with primary antibody, anti-p53 DO-7 (1:200, DAKO) incubation was carried out at room temperature for 30 min and samples were incubated with HRP-conjugated antibody from the LSAB-Plus/HRP kit (Dako). Nuclei were counterstained with haematoxylin. p53 staining was evaluated using a DM1000 microscope (Leica). Nuclear p53 localization was measured as percentage of cells. For each sample, 50 randomly selected regions were analysed and compared with the staining in its normal tissue.

Mouse strains and animal care. P53 R172H/R172H, $p53^{-/-}$ and $p53^{+/+}$ genotypes were maintained on a C57BL/6 background and genotyping was performed by polymerase chain reaction (PCR) analysis as described previously[8]. Female animals showing signs of illness or evident tumour burden were euthanized and organs frozen on extraction in liquid nitrogen for −80 °C storage until protein extraction for the proteasome activity assay and western blot.

For *in vivo* xenograft studies we used SCID CB17 female mice (Charles River Laboratories) aged 7 weeks.

Procedures involving animals and their care were in conformity with institutional guidelines (D.L. 116/92 and subsequent complementing circulars); all experimental protocols were approved by the ethical Committee of the University of Padua (CEASA) and conducted according to the UK Coordinating Committee on Cancer Research (UKCCCR) guidelines of 1989 for the welfare of animals in experimental neoplasia. During *in vivo* experiments, animals in all experimental groups were examined daily for a decrease in physical activity and other signs of disease.

***In vivo* xenograft experiments.** For *in vivo* tumour growth and metastasis assays MDA-MB-231 cells were transduced with a lentiviral vector coding for the firefly luciferase reporter gene.

For MDA-MB-231 xenograft experiments, 1×10^6 cells were resuspended in 100 µl of DMEM, and injected into the mammary fat pad of previously anaesthetized (1–3% isoflurane, Merial Italia) SCID mice. For the MCF7 xenograft experiment, 10×10^6 cells were resuspended in 100 µl of DMEM, and injected into the mammary fat pad of SCID female mice anaesthetized as above. For MCF7 cells, mice were injected once a week intramuscularly with 1 mg kg^{-1} oestradiol cypionate in cottonseed oil (solution 1 mg ml^{-1} prepared from Sigma reagents). Tumour growth at the injection sites was monitored by calliper measurements.

We performed *in vivo* imaging at 9–37 days after the subcutaneous fat pad injection, in 7-day intervals. Anaesthetized animals were given the substrate D-luciferin (PerkinElmer) by intraperitoneal injection at 150 mg kg^{-1} in PBS (Sigma). The light emitted from the bioluminescent tumours or metastasis was detected using the IVIS Lumina II Imaging System (Calliper Life Sciences). Regions of interest from displayed images were quantified as total photon counts or photon/s using Living Image software (Xenogen).

Primary tumours were extracted at 5 weeks post treatment initiation for treatment controls and after reaching a comparable size in mice treated with drugs. Tumours were frozen in liquid nitrogen for molecular analyses. Lymph nodes and lungs were excised, formalin-fixed and paraffin-embedded for haematoxylin–eosin staining and human cytokeratin 7 (Cell Marque, OV-TL12/30) immunohistochemistry.

Animal groups and drug administration. Experiment 1, MDA-MB-231: 36 SCID mice, 6 groups of 6 mice, 4 weeks, drugs administered 2× a week intravenously with a 2-day interval, drugs mixed before administration (when needed) in final injection volume of 200 µl PBS. Groups: DMSO (Ctrl), CFZ (carfilzomib, Selleckchem; 1.5 mg kg^{-1}), PRIMA-1 (Tocris Bioscience; 50 mg kg^{-1}), CFZ (1.5 mg kg^{-1}) + PRIMA-1 (50 mg kg^{-1}), SAHA (Tocris Bioscience; 50 mg kg^{-1})—2 animals deceased at 2 weeks, CFZ (1.5 mg kg^{-1}) + SAHA (50 mg kg^{-1})—2 animals deceased at 2 weeks. Four mice in each group were selected for the final result.

Experiment 2, MDA-MB-231: 36 SCID mice, 4 groups of 9 mice, 5–7 weeks, CFZ administered intravenously 2× a week with a 2-day interval, APR-246 (PRIMA-1 MET, provided by Aprea, Karolinska Institutet Science Park) administered intravenously 3× a week on days alternating the CFZ injection (drugs were not mixed on administration), injection in 200 µl PBS. Groups: DMSO (Ctrl), CFZ (1.5 mg kg^{-1}), APR-246 (100 mg kg^{-1}), CFZ (1.5 mg kg^{-1}) + APR-246 (100 mg kg^{-1}). Eight mice in each group were selected for the final results; *ex vivo* molecular studies were performed in the biopsy material from five mice from the selected groups.

Experiment 3, MCF7: 14 SCID mice, 2 groups of 7 mice, 5 weeks, CFZ administered intravenously 2× a week with a 2-day interval, APR-246 (PRIMA-1 MET, provided by Aprea, Karolinska Institutet Science Park) administered intravenously 3× a week on days alternating the CFZ injection (drugs were not mixed on administration), injection in 200 µl PBS: CFZ (1.5 mg kg^{-1}) + APR-246 (100 mg kg^{-1}). Six mice in each group were selected for the final results.

Data availability. Data that support the findings of this study have been deposited in the Gene Expression Omnibus (GEO) under accession codes GSE65458 (Microarrays), GSE68248 (RNA-seq) and GSE66543 (ChIP-seq). The proteomics data were deposited in the PRIDE repository under accession code PXD001673 (file Dawid1.zip contains the MDA-MB-231 siRNA TP53 experiment: A1–4 are four replicates of the siRNA TP53 condition; B1–4 are four replicates of the siRNA control condition, file Dawid2.zip contains the MDA-MB-231 siRNA PSMA2 experiment: A1–4 are four replicates of the siRNA PSMA2 condition; B1–4 are four replicates of the siRNA control condition). Source data for Fig. 1 and Supplementary Fig. 1 (gene/protein signatures, proteomics, transcriptomics, ChIP-seq peaks, pathway analysis, proteasome transcription validation) have been provided as Supplementary Tables 1–5, 9 and 13. Source data for Fig. 3b and Supplementary Fig. 3d (human tumour samples) have been provided as Supplementary Table 15. Source data for Fig. 4 and Supplementary Fig. 4 (ChIP validation, TF identification) have been provided as Supplementary Tables 4 and 6. Source data for Fig. 6 and Supplementary Fig. 6 (protein signature, proteomics) have been provided as Supplementary Tables 1 and 2.

Gene expression data, *TP53* mutation status and clinical annotation for Breast Invasive Carcinoma, Bladder Carcinoma, Lung Adenocarcinoma, Head and Neck Carcinoma, Colorectal Adenocarcinoma, Urothelial Bladder Cancer, Brain Lower Grade Glioma, Liver Hepatocellular Carcinoma, Squamous Cell Lung Cancer (TCGA data sets) for Fig. 2b and Supplementary Fig. 2d and Supplementary Table 14 were obtained from the Cancer Genomics Data Server using the cgdsr package for R.

The breast cancer patient survival data for Fig. 2a and Supplementary Fig. 2a,c were derived from a breast cancer meta-data set composed of 3,458 samples associated with the Km-plotter online analysis tool. Expression and clinical data of breast cancer samples in this meta-data set were obtained from the following data sets: E-MTAB-365, GSE11121, GSE12093, GSE12276, GSE1456, GSE16391, GSE16446, GSE17705, GSE17907, GSE19615, GSE20194, GSE20271, GSE2034, GSE20685, GSE20711, GSE21653, GSE2603, GSE26971, GSE2990, GSE31448, GSE31519, GSE3494, GSE5327, GSE6532, GSE7390, GSE919.

Data used to calculate statistics in Figs 1d, 3a,c–f, 4d–g, 5d, 6e,h,i, 7b and Supplementary Figs 1e, and 3a–c,e–h, 4c,d, 5d,g, 6a,e,h and 7a,b,d–g are provided in Supplementary Table 10 (Statistics source data). All other data supporting the findings of this study are available from the corresponding author on request.

67. Kuhn, M. Building predictive models in R using the caret package. *J. Stat. Softw.* **28,** 1–26 (2008).
68. Bindea, G. *et al.* ClueGO: a Cytoscape plug-in to decipher functionally grouped gene ontology and pathway annotation networks. *Bioinformatics* **25,** 1091–1093 (2009).
69. Warde-Farley, D. *et al.* The GeneMANIA prediction server: biological network integration for gene prioritization and predicting gene function. *Nucleic Acids Res.* **38,** W214–W220 (2010).
70. Gostissa, M. *et al.* The transcriptional repressor hDaxx potentiates p53-dependent apoptosis. *J. Biol. Chem.* **279,** 48013–48023 (2004).

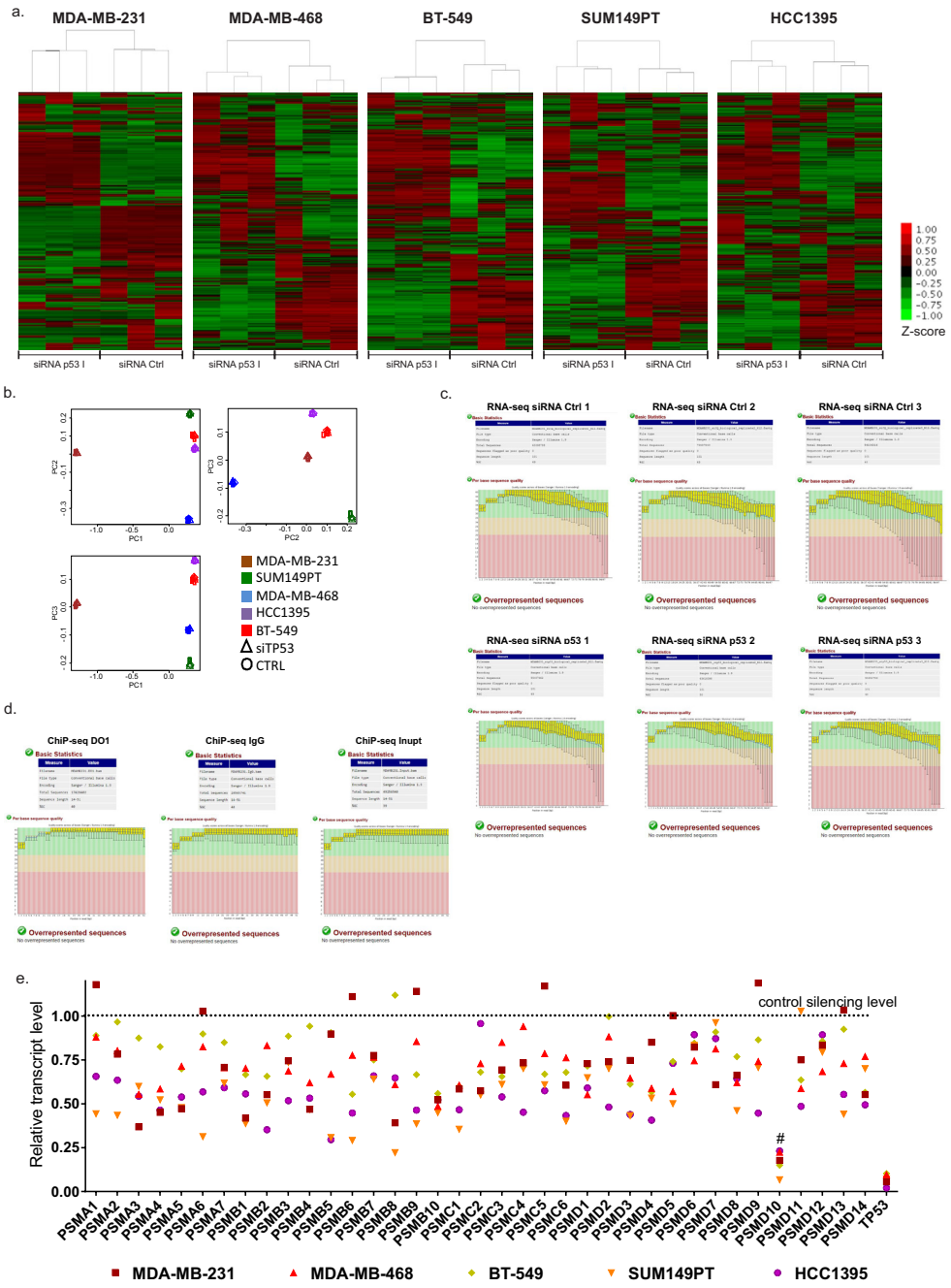

Supplementary Figure 1 a. Hierarchical clustering of gene expression data for each of the TNBC cell lines shown in Fig. 1b. In each expression matrix, after Z-score standardization, the genes with low standard deviation were filtered (MDA-MB-231: Genes 16804 (sd filter =0.05), MDA-MB-468: Genes 11428 (sd filter =0.1), BT-549: Genes 17531 (sd filter =0.1), SUM149PT: Genes 14125 (sd filter =0.1), HCC1395: Genes 10432 (sd filter =0.1)). Increased (red) or decreased (green) expression of the genes is shown for each sample. Bars below the graphs identify the samples subjected to Control (Ctrl) or TP53 (p53) silencing (n=3 for each cell line and condition); b. Principal component analysis (PCA) was performed on the five cell lines expression matrix. The first 3 principal components are plotted in pairs, the emerging sample groups confirmed that each cell line is a homogeneous cell population irrespective of being silenced for TP53 (triangles) or not (circles). The difference among the cell lines is larger than between the controls and the TP53 silencing; c. MDA-MB-231 cells RNA-seq samples quality control performed using FastQC. Selected results are shown. d. MDA-MB-231 cells ChIP-seq samples quality control performed using FastQC. Selected results are shown. e. Extended result from Figure 1d: transcript levels of all human 26S proteasome and immunoproteasome subunits determined in five TNBC cell lines upon mutant TP53 expression silencing using alternative siRNA – 3'UTR-targeting siRNA II (normalized control level shown as the dashed line, each result is a mean of two independent experiments). # marks a possible off-target effect of TP53 siRNA II towards PSMD10 transcript. For individual expression values of each gene in each cell line, see Supplementary Tab. 3. Statistics source data for 1e provided in Supplementary Table 10.

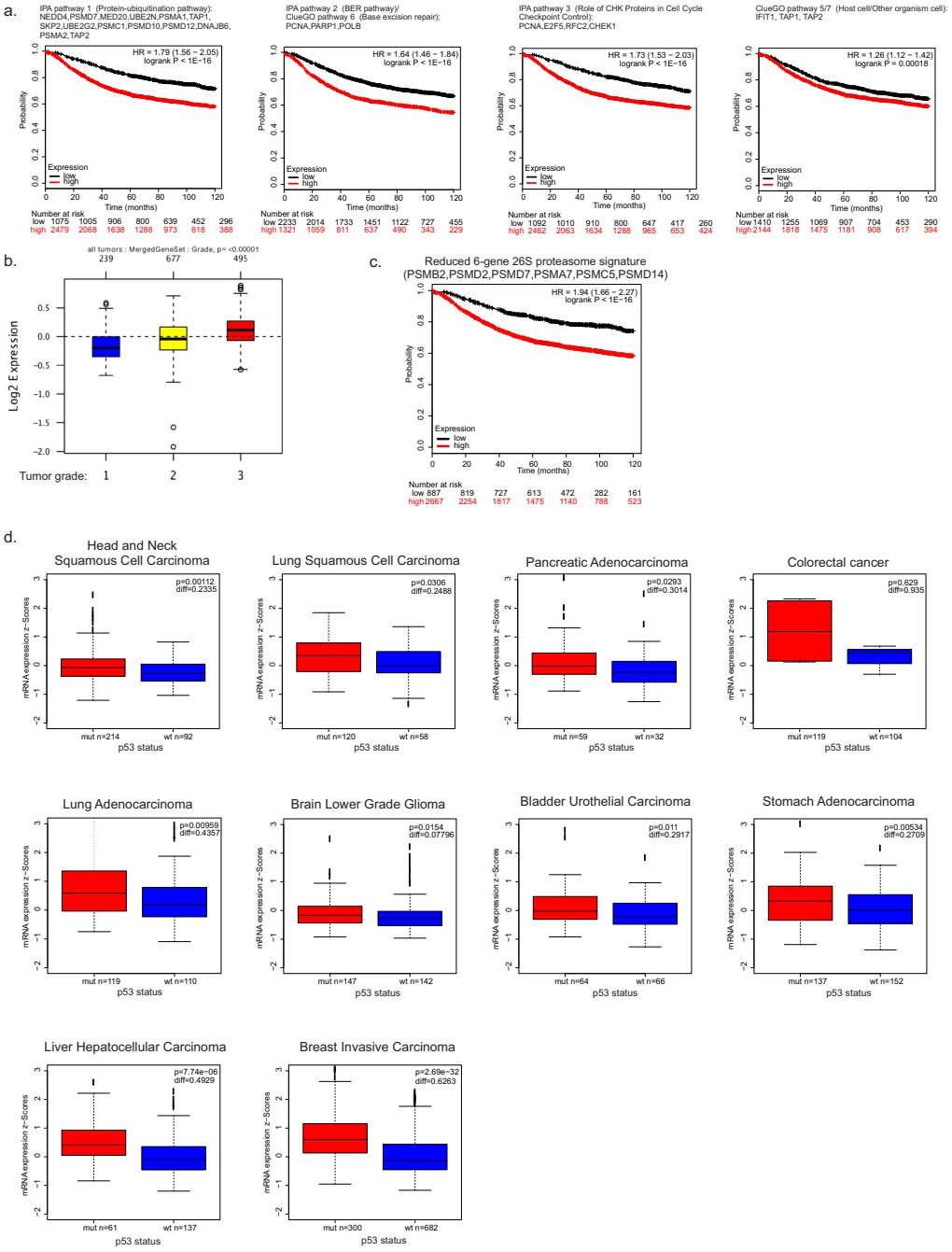

Supplementary Figure 2 a. The mutant p53-related proteasome-ubiquitination pathway gene expression is more significantly associated with poor prognosis in breast cancer patients than of the genes from other top pathways derived from the common mutant p53 signature. HR – hazard ratio; logrank P – logrank test p-value for the curves comparison (n=3458); b. The high expression of 37 proteasome genes ("whole proteasome signature") is associated with the high grade of breast cancer in patients (grades marked 1-3). P-value is derived from Mann–Whitney U test (n=1401). Box plot centre represents the median, box extremes indicate first and third quartile, whiskers extend to the extreme values included in the interval calculated as +/-1.58 IQR/sqrt(n) where IQR (interquartile range) is calculated as the third quartile minus the first quartile.; c. The best recursive feature selection analysis scoring proteasome gene subset (composed of 6 genes, see Methods and Supplementary Table 8) was evaluated for the prognostic correlation in the breast cancer dataset (survival graph as in a.; HR – hazard ratio; logrank P – logrank test p-value for the curves comparison, n=3458).; d. The high expression of 37 proteasome genes is associated with the mutant TP53 status in the indicated cancer types (diff – difference in mean signature expression in mutant vs wt p53 status samples; p-value is derived from Mann–Whitney U test). Number of patients for each cancer type is indicated below each graph, based on selection in Supplementary Table 14. Box plot centre represents the median, box extremes indicate first and third quartile, whiskers extend to the extreme values included in the interval calculated as +/-1.58 IQR/sqrt(n) where IQR (interquartile range) is calculated as the third quartile minus the first quartile.

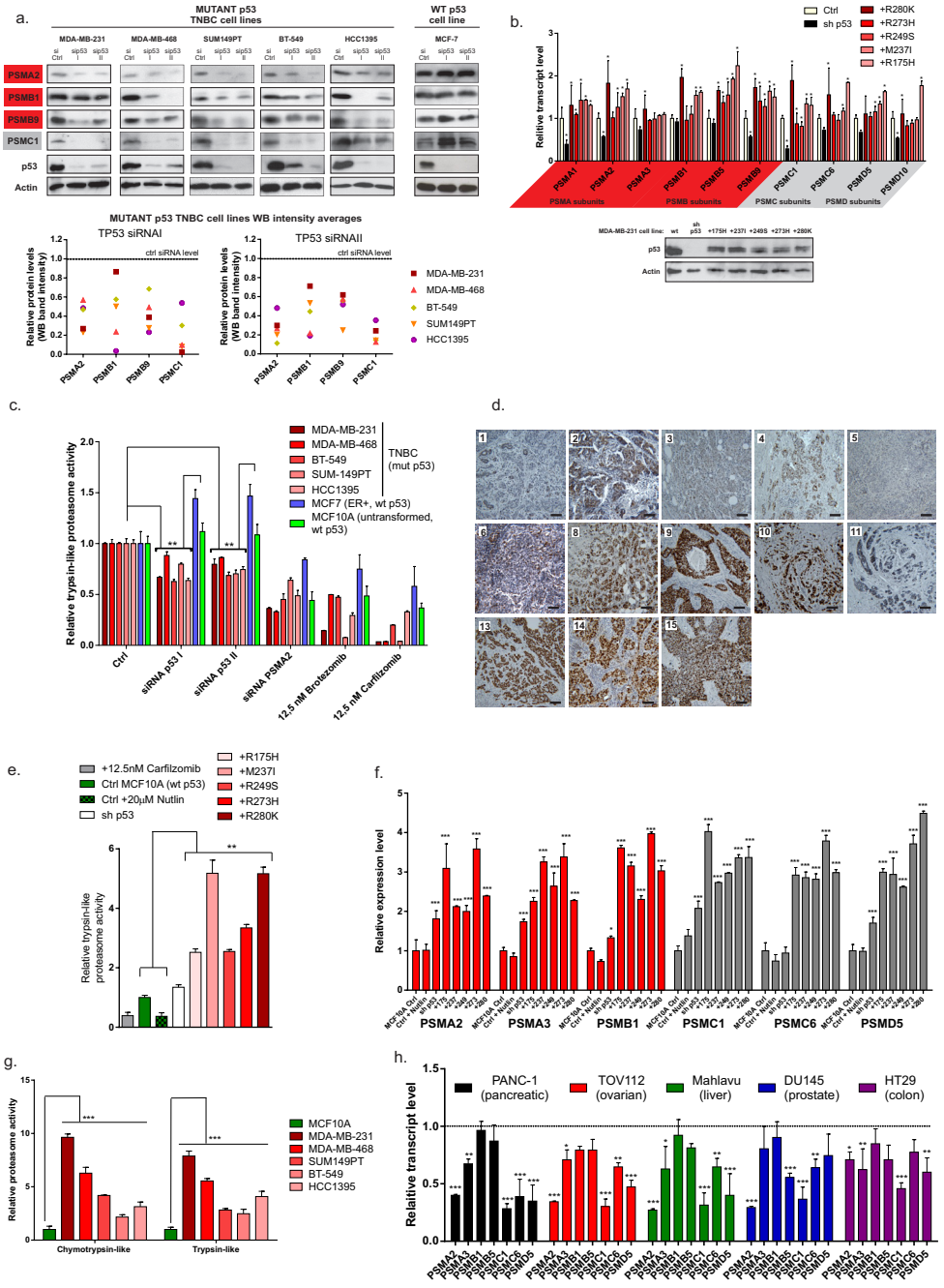

Supplementary Figure 3 a. Levels of selected proteasome subunits are lowered upon TP53 expression silencing in the 5 TNBC cell lines. Below – a bar graphs demonstrating protein levels of proteasome subunits measured by densitometry in 5 TNBC cell lines with mutant p53 (averages of two western-blots per each result are used; two alternative siRNAs – TP53 siRNA I and II; normalized control silencing level shown as the dashed line); b. Overexpressed mutant p53 variants rescue proteasome genes transcription in the stably silenced endogenous mutant TP53 background of MDA-MB-231 cells. Lower panel: western blot demonstrating stable silencing of mutant TP53 and expression of the mutant p53 variants (representative of 2 repeats); c. Trypsin-like proteasome activity is decreased in mutant p53 TNBC cell lines versus wt p53 cell lines (MCF10A and MCF7) upon silencing of mutant TP53 or PSMA2 or proteasome inhibitor treatment (24h; Carfilzomib, Bortezomib).; d. IHC staining of p53 (brown) in representative samples from Fig. 3b with indicated numbers corresponding to the Supplementary Table 15; Scale bars are 100μM; e. Trypsin-like proteasome activity in MCF10A cell lines treated with 20μM Nutlin for 24h, stably transfected with vector encoding shRNA targeting TP53 and indicated mutant p53 cds shRNA-resistant HA-tagged variants (+p53 changed residue); f. Transcript levels of proteasome subunits in MCF10A cell lines treated with 20μM Nutlin for 24h, stably transfected with vector encoding shRNA targeting TP53 and indicated mutant p53 cds shRNA-resistant HA-tagged variants (+p53 changed residue); g. Basal chymotrypsin-like and trypsin-like proteasome activities are elevated in the TNBC cell lines (mutant p53), as compared to the MCF10A cell line (wt p53).; h. Transcript levels of proteasome subunits are decreased in the indicated non-breast cancer cell lines upon mutant TP53 expression silencing. Control level is marked with the dashed line. b-c, e-h: Means of n=3 biologically independent samples with s.d. are shown, ANOVA test with Bonferroni correction: * $p<0.05$, ** $p<0.01$, *** $p<0.001$; Unprocessed scans of blots are shown in Supplementary Fig. 9. Statistics source data for 3a-c, e-h provided in Supplementary Table 10.

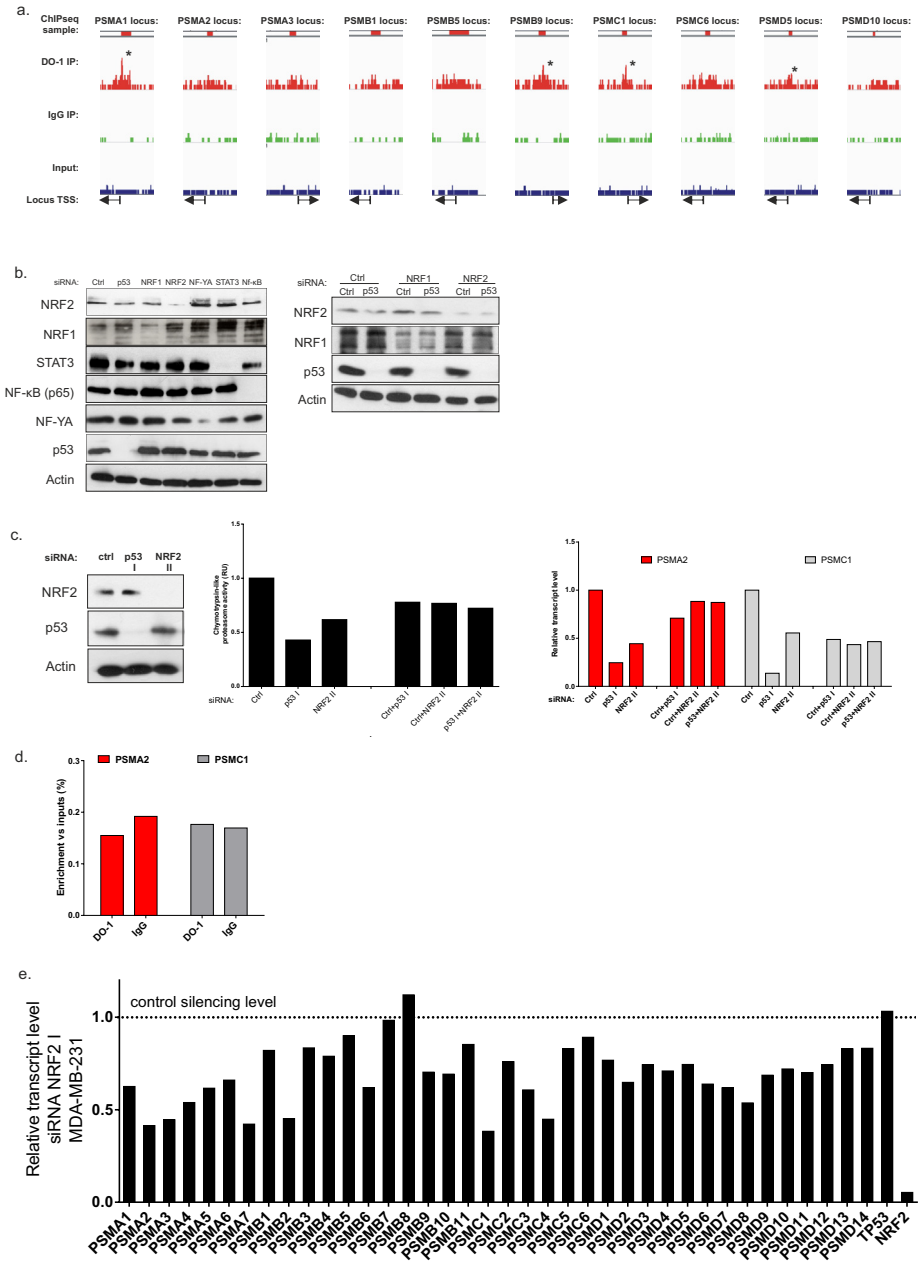

Supplementary Figure 4 a. Integrative Genomics Viewer (IGV) snapshots at the selected proteasome subunit gene loci with shown ChIP-sequencing enrichment readouts for the indicated samples in the MDA-MB-231 cells – DO-1 p53 ChIP (red), IgG ChIP (green), ChIP input (blue). (*) indicate significant peaks called in range -+500 bp of proteasome gene TSSes (Supplementary Tab. 4), other peak regions were hand-picked in IGV. Regions highlighted in red were used to design mutant p53 binding-region region primers for ChIP validation shown in Figure 4a (primers listed in the Supplementary Tab. 7); b. Western blot related to Figure 4c (left panel) and Figure 4d (right panel) showing protein levels of the transcription factors whose expression has been silenced in the indicated samples (representative of 3 repeats); c. Effects of transfection of alternative siRNA for NRF2 (NRF2 II) and siRNA for TP53 on proteasome activity (middle panel) and transcription (right panel) are comparable with siRNA NRF2 I treatment shown in Figure 4c and 4d. Means of data from two independent experiments; d. Chromatin immunoprecipitation enrichment obtained with the indicated antibodies at PSMA2 and PSMC1 mutant p53 binding regions in the wt p53 MCF7 cells – no enrichment increase is observed for DO-1 ChIP. Means of data from two independent experiments; e. Transcript levels of all human 26S proteasome and immunoproteasome subunits determined in MDA-MB-231 cells upon mutant NRF2 expression silencing (normalized control level shown as the dashed line, means of data from two independent experiments). For individual expression values of each gene see Supplementary Tab. 5. Unprocessed scans of blots are shown in Supplementary Fig. 9. Statistics source data for 4c-d provided in Supplementary Table 10.

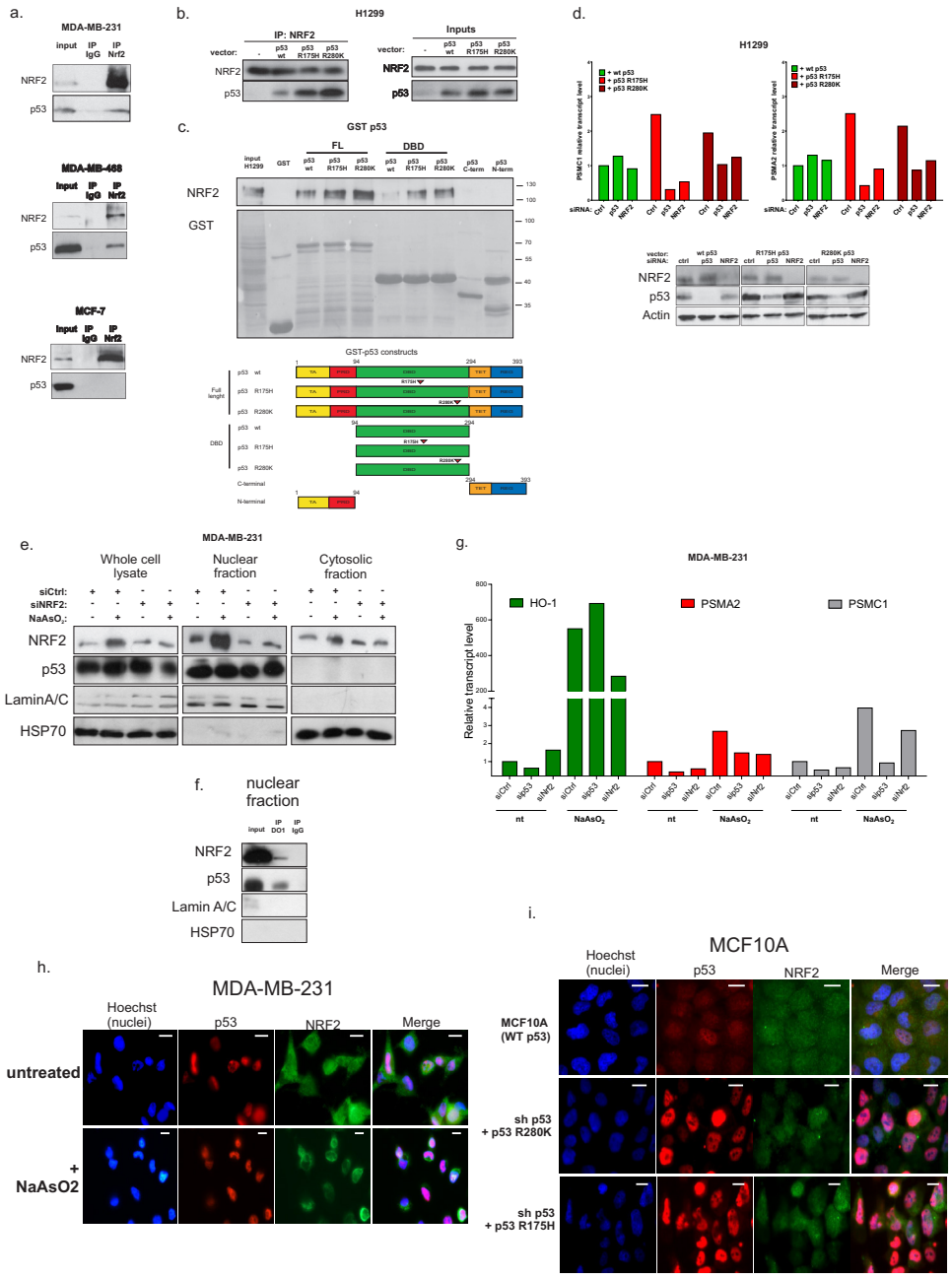

Supplementary Figure 5 a. Mutant p53 co-immunoprecipitates (co-IP) with Nrf2 in MDA-MB-231 and MDA-MB-468 cell lysates but not in MCF-7 cell lysate (anti-Nrf2 antibody). Representative of 2 repeats; b. Co-immunoprecipitation (co-IP) of Nrf2 (anti-Nrf2 antibody) and overexpressed wt or mutant (R175H and R280K) p53 in p53-null H1299 cells (representative of 2 repeats); c. GST tagged mutant p53 variants (E.coli overexpressed) interact via DNA binding domain with overexpressed full length Nrf2 in the p53-null H1299 cell lysates. (FL- full length protein; DBD – DNA binding domain; N-term – amino terminal domain; C-term – carboxy terminal domain of p53). Below a ponceau-red stained membrane is shown with transferred GST-fusion constructs (representative of 3 repeats) and a scheme of the N-terminally GST-tagged p53 constructs used for the experiment; d. The increased expression of PSMA2 and PSMC1 proteasome genes is blunted by silencing of TP53 or NRF2 in the presence of the overexpressed mutant p53 variants (R175H and R280K) in p53-null H1299 cells. The effect is absent in the wt p53 overexpressing cells (means of two independent experiments). Below – a western blot showing p53 and Nrf2 levels in H1299 upon indicated silencing (representative of 2 repeats); e. Nrf2 and p53 are present in the nuclei of MDA-MB-231 cells with or without oxidative stress. Cells optionally treated with Nrf2-targeting siRNA and/or for 6h with 50 μM of oxidative stress-inducing sodium arsenite (NaAsO2). Representative of 3 repeats; f. Mutant p53 co-immunoprecipitates with Nrf2 in the nuclear fraction of MDA-MB-231 (representative of 3 repeats); g. Mutant p53 regulates transcription of Nrf2-dependent oxidative stress induced gene HO-1 in the opposite manner to the proteasome genes. Means of two independent experiments. h. Nrf2 and p53 co-localize in the nuclei of MDA-MB-231 with or without oxidative stress. Cells optionally treated for 6h with 50 μM of oxidative stress-inducing sodium arsenite (NaAsO2). Representative of 3 repeats); i. Nrf2 and p53 co-localize in the nuclei of MCF10A control cells (wt p53) and MCF10A cells with silenced endogenous wt TP53 (sh p53) plus overexpressed mutant p53 variants (+p53 R280K. +p53 R175H). Representative of 3 repeats. Unprocessed scans of blots are shown in Supplementary Fig. 9. Statistics source data for 5d, g provided in Supplementary Table 10.

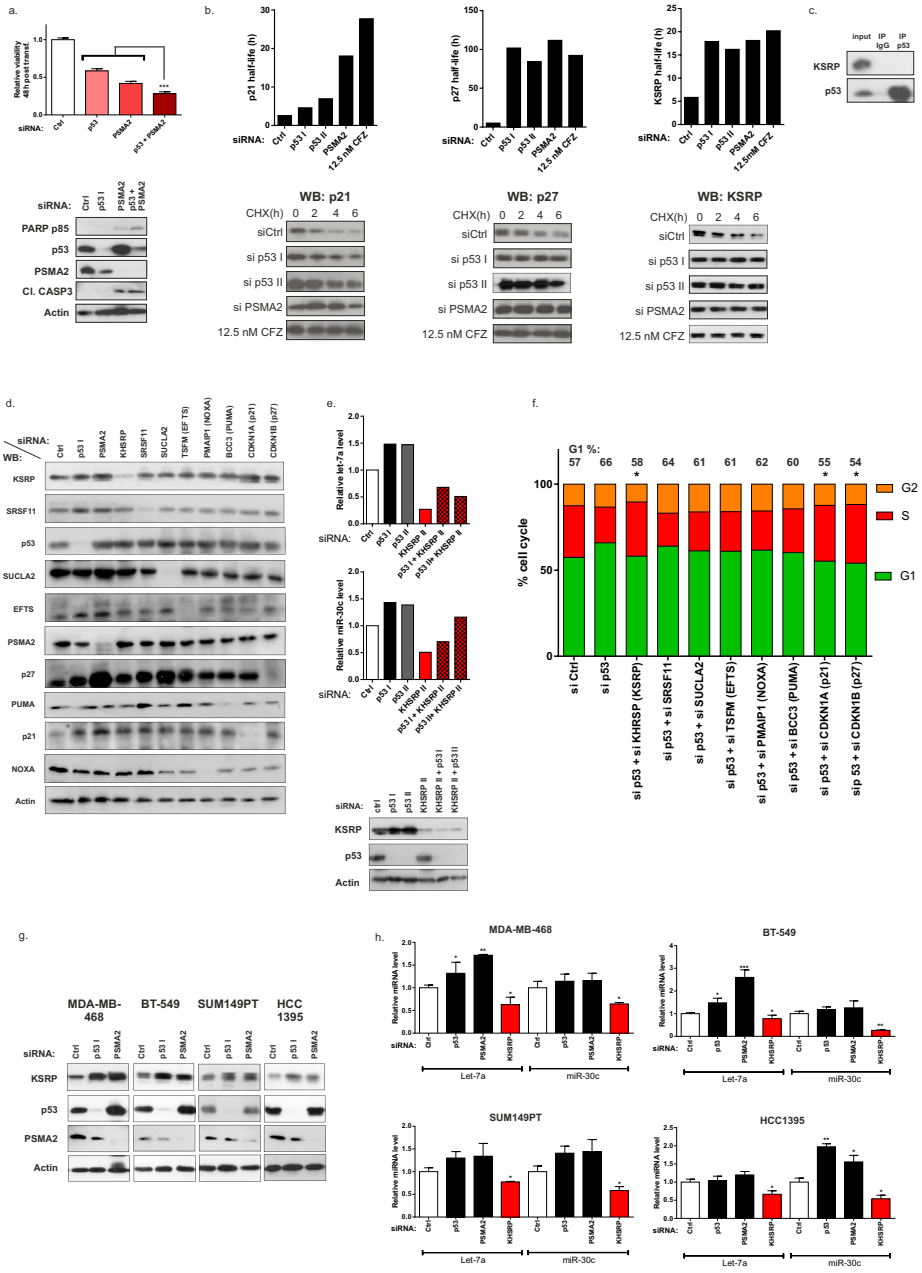

Supplementary Figure 6 a. Simultaneous silencing of mutant TP53 and essential proteasome subunit PSMA2 concomitantly decreases MDA-MB-231 cells viability and induces apoptosis markers. Bar graph represents cell viability 48 hours post silencing of mutant TP53, PSMA2 or both. Means of n=4 biologically independent samples are shown with s.d., ANOVA test with Bonferroni correction: *** p<0.001. Lower panel: western blot showing the silencing effects on p53/PSMA2 and induction of apoptosis markers: PARP p85 fragment and cleaved Caspase 3 (representative of 3 repeats).; b. Protein stability of proteasome target proteins p21, p27, KSRP is increased upon silencing of TP53, PSMA2 or treatment with the proteasome inhibitor Carfilzomib (CFZ) in MDA-MB-231 cells (half-lives and western blots are representatives of 2 repeats are shown); c. KSRP protein does not interact with mutant p53 in MDA-MB-231 cells (representative of 2 repeats); d. Protein levels of mutant p53-proteasome axis targets, upon their silencing as described in Figure 6 c-e (representative of 3 repeats); e. Effects of alternative siRNAs used for KHSRP and mutant TP53 silencing on the levels of oncosuppressive microRNAs (bar graphs). Means of two independent experiments; f. Silencing of KHSRP (KSRP), CDKN1A (p21), CDKN1B (p27) suppresses cell cycle arrest induced by mutant TP53 knockdown in MDA-MB-231 cells. Additional silencing of KHSRP (KSRP), CDKN1A (p21) or CDKN1B (p27) most efficiently restores the normal cell cycle profile (marked with *). Representative of 3 repeats; g. Mutant TP53 or PSMA2 silencing induces KSRP protein level increase in the TNBC cell lines. Representatives of 2 repeats for each cell line; h. Mutant TP53 or PSMA2 silencing induces levels of oncosuppressive microRNAs Let-7a and miR30c, while silencing of KHSRP reduces them in the indicated TNBC cell lines. Means of n=3 biologically independent samples are shown with s.d., ANOVA test with Bonferroni correction: * p<0.05, ** p<0.01, *** p<0.001; Unprocessed scans of blots are shown in Supplementary Fig. 9. Statistics source data for 6a, e, h provided in Supplementary Table 10.

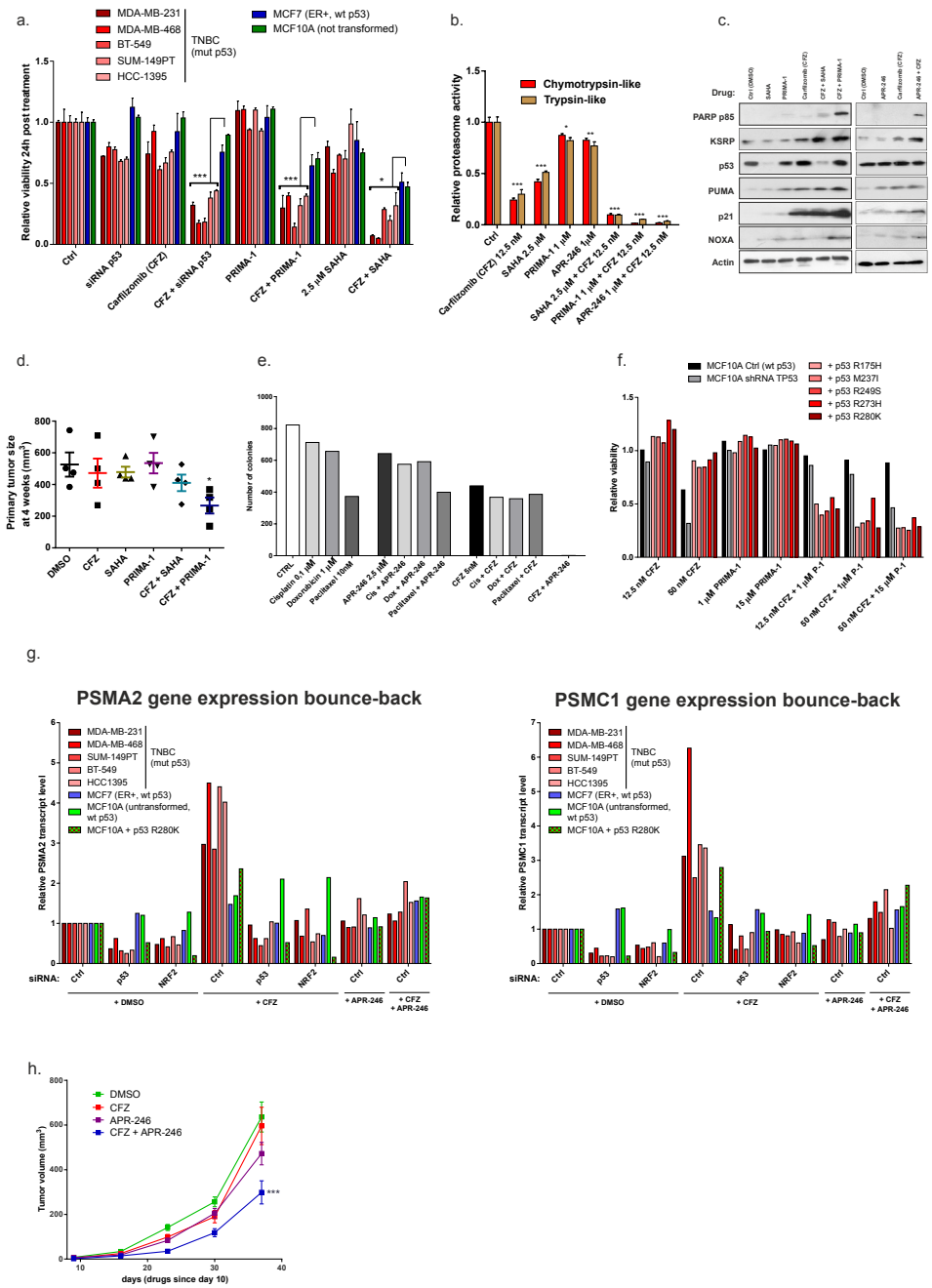

Supplementary Figure 7 a. TP53 silencing or targeting with SAHA (Vorinostat) or PRIMA-1 sensitizes TNBC but not wt p53 cell lines to the proteasome inhibitor Carfilzomib (CFZ). Viability post 24h treatment is shown. b. Drug-mediated inhibition of proteasome and mutant p53 synergistically decreases the proteasome activity in MDA-MB-231 cells. c. 24h treatment of MDA-MB-231 cells with SAHA (2,5 μM), PRIMA-1 (1 μM) or APR-246 (1 μM) plus the proteasome inhibitor Carfilzomib (CFZ; 12.5 nM) induces tumor suppressive proteins KSRP, PUMA, p21 and NOXA (latter 3 are wt p53 targets) and the apoptosis marker PARP p85 increase. Representative of 2 repeats; d. Simultaneous administration of PRIMA-1 and the proteasome inhibitor Carfilzomib (CFZ) inhibits the growth of primary xenograft tumors more effectively than a combination of SAHA and CFZ. Means of n=4 animals with s.e.m. are shown, ANOVA test with Bonferroni correction: * p<0.05, ** p<0.01, *** p<0.001; e. Concomitant treatment of MDA-MB-231 cells with Carfilzomib (CFZ) and APR-246 eliminates Carfilzomib resistant colonies while combining CFZ or APR-246 Cisplatin, Doxorubicin or Paclitaxel does not increase their toxicity. Means of two independent experiments; f. Introduction of mutant p53 variants to MCF10A cells with stably silenced wt p53 increases their resistance to proteasome inhibitor Carfilzomib (CFZ) but sensitizes them to the CFZ+APR-246 combination (viability, 24h treatment). Means of two independent experiments; g. Mutant TP53, NRF2 silencing or APR-246 (PRIMA-1MET) treatment reduces the proteasome genes PSMA2 (left graph) and PSMC1 (right graph) transcript increase due to the bounce-back effect post treatment with Carfilzomib (CFZ) in TNBC cell lines. Means of of two independent experiments; h. Primary MDA-MB-231-Luc (mutant p53, TNBC) subcutaneous xenograft growth in SCID mice is significantly reduced compared to the DMSO (caliper measurement, means of n=8 independent animals with s.e.m. are shown, significance for the time-course is indicated - Friedman nonparametric matched pairs test with Dunn's correction; *** p<0.001). a-b: Means of n=3 biologically independent samples with s.d. are shown, ANOVA test with Bonferroni correction: * p<0.05, ** p<0.01, *** p<0.001; Unprocessed scans of blots are shown in Supplementary Fig. 9. Statistics source data for 7a-b, d-g provided in Supplementary Table 10.

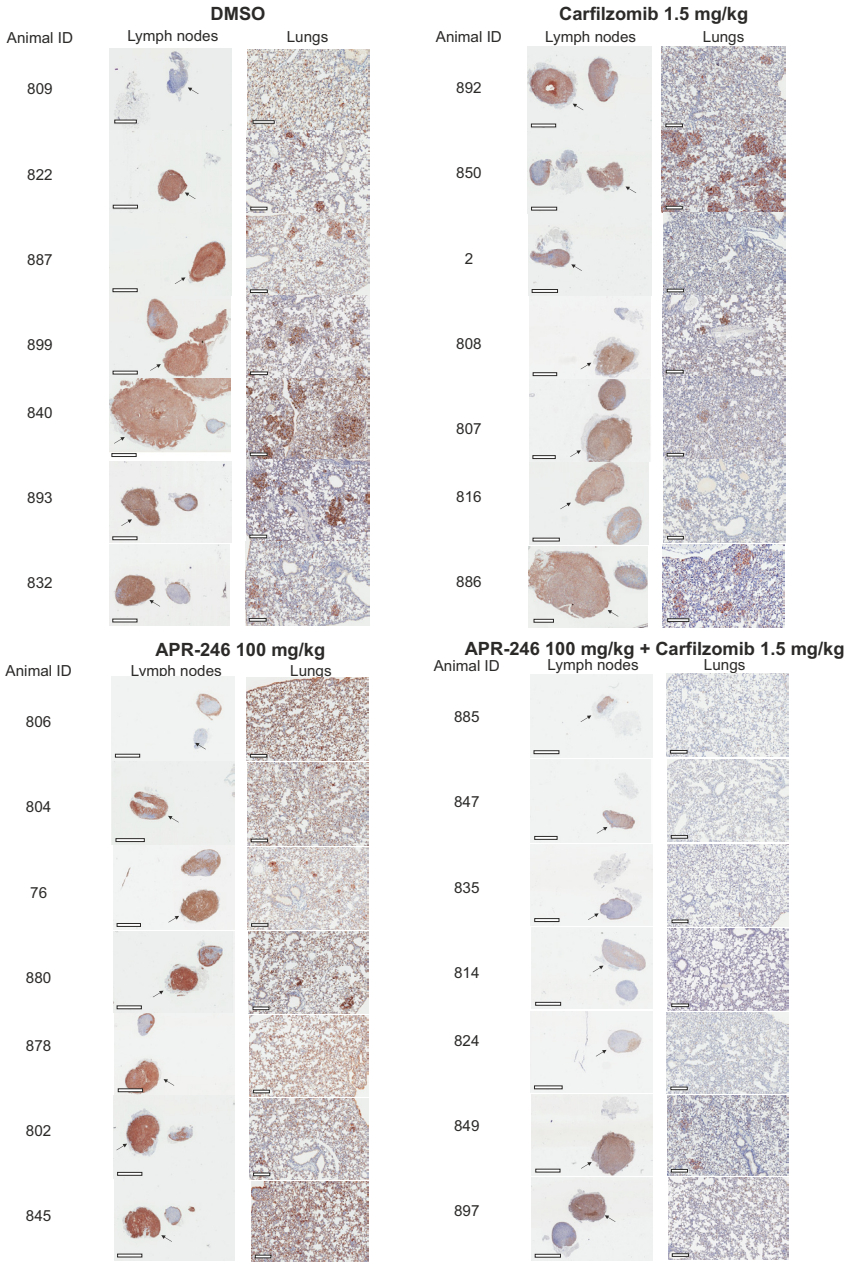

Supplementary Figure 8 Treatment of SCID mice with MDA-MB-231 cells-derived xenografts tumors using the combination of APR-246 (PRIMA-1MET) and Carfilzomib (CFZ) strongly reduces metastasis to lymph nodes and lungs. Photos of the tissue slices of lymph nodes (lymph nodes homolatreal to xenogafts - indicated by arrows; bar size – 2 mm) and lungs (bar size – 200 µm) with MDA-MB-231 metastasis IHC staining (human cytokeratin, brown) from remaining mice in the experiment shown in Figure 7g.

Fig. 3c:

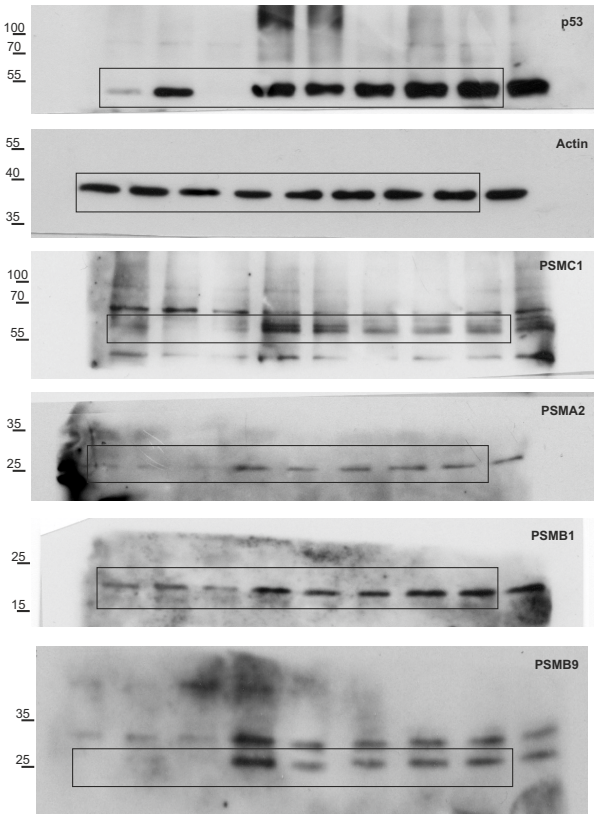

Fig. 3e:

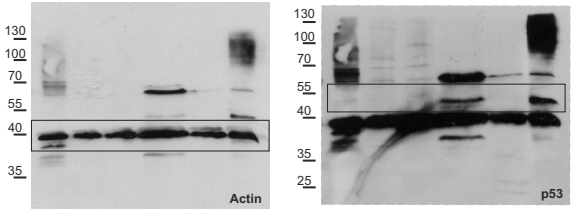

Fig. 3f:

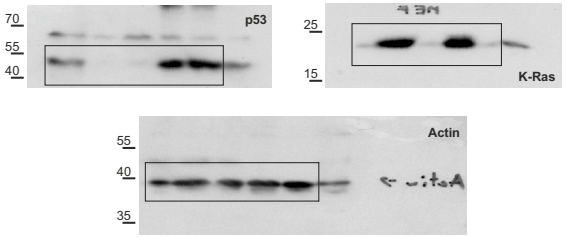

Fig. 5b:

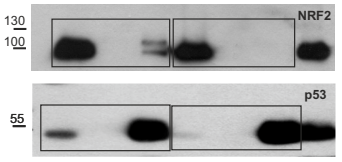

Fig. 5c:

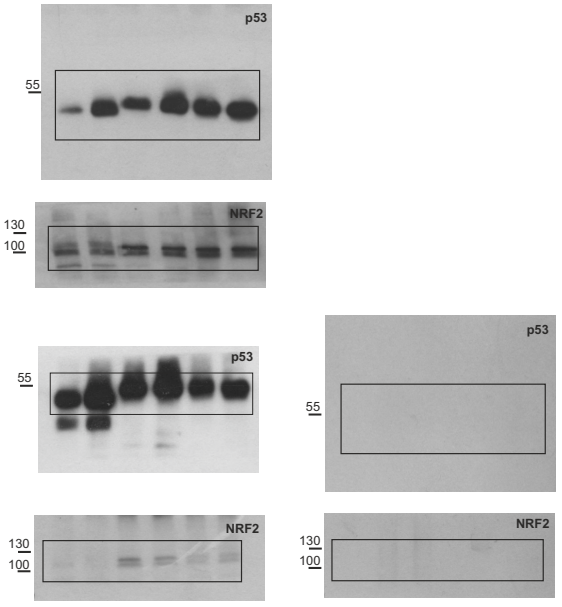

Fig. 5d:

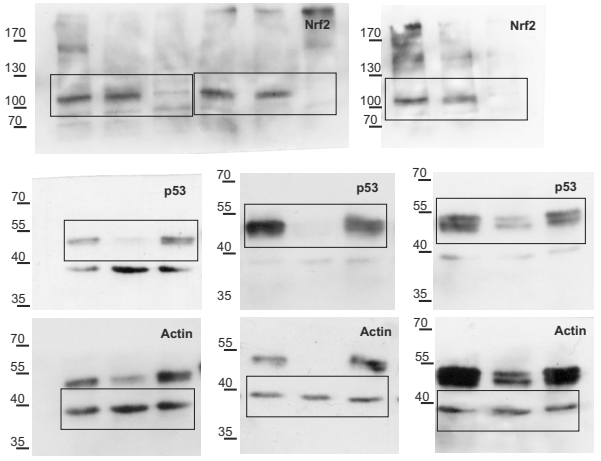

Supplementary Figure 9 Scans of developed films with approximate regions used for figures marked with rectangles and molecular sizes indicated in kDa (based on prestained protein markers).

Fig. 5a

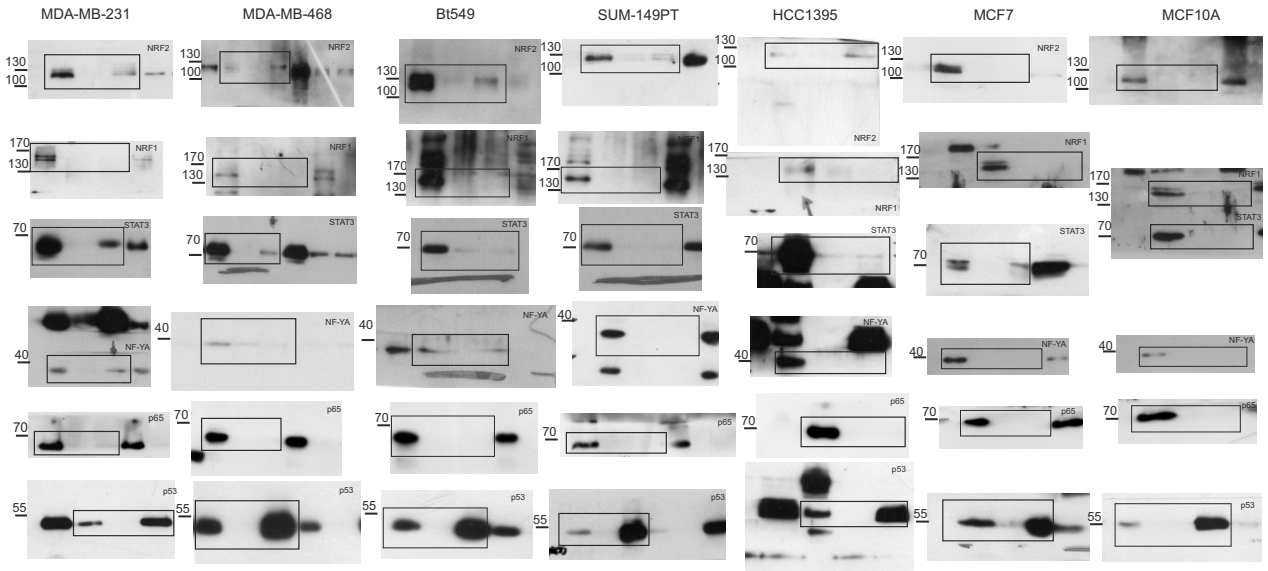

Fig. 7k:

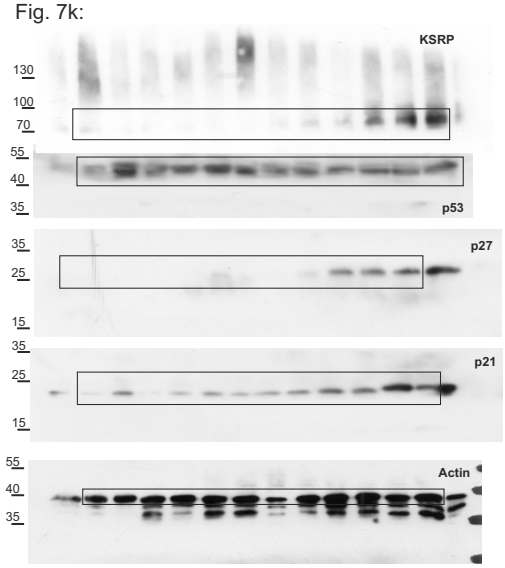

Fig. 6f:

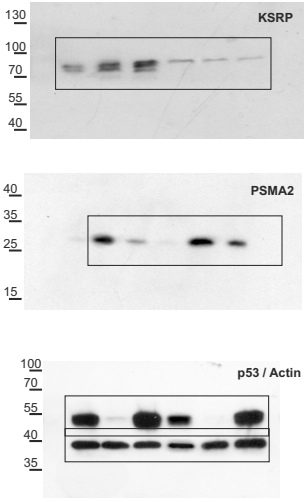

Supplementary Figure 9 continued

Supp. Fig. 3a:

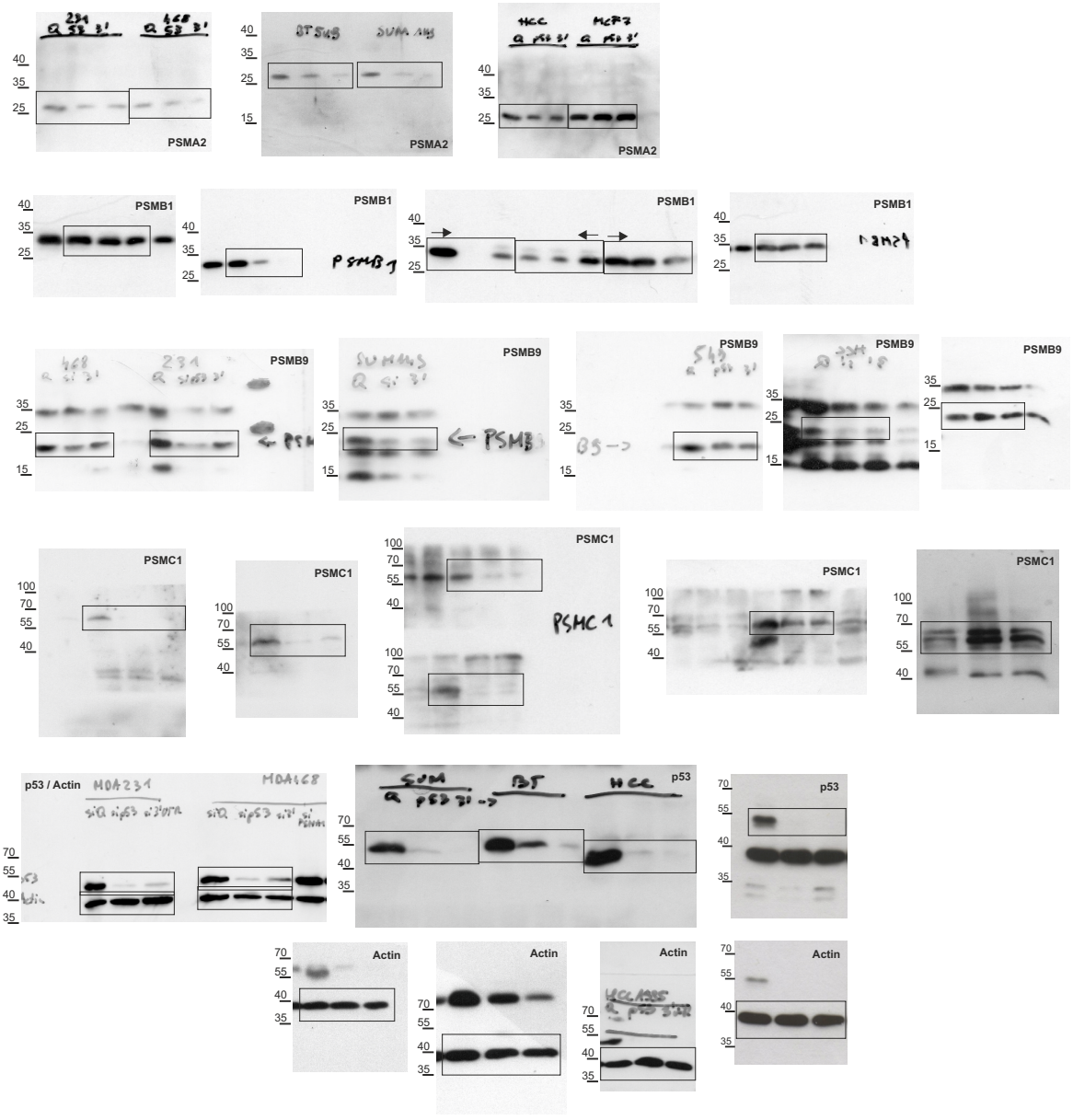

Supp. Fig. 3b:

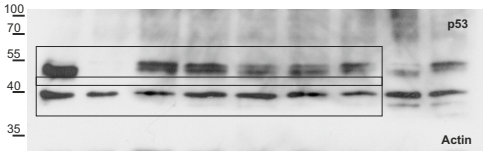

Supplementary Figure 9 continued

Supp Fig. 4b:

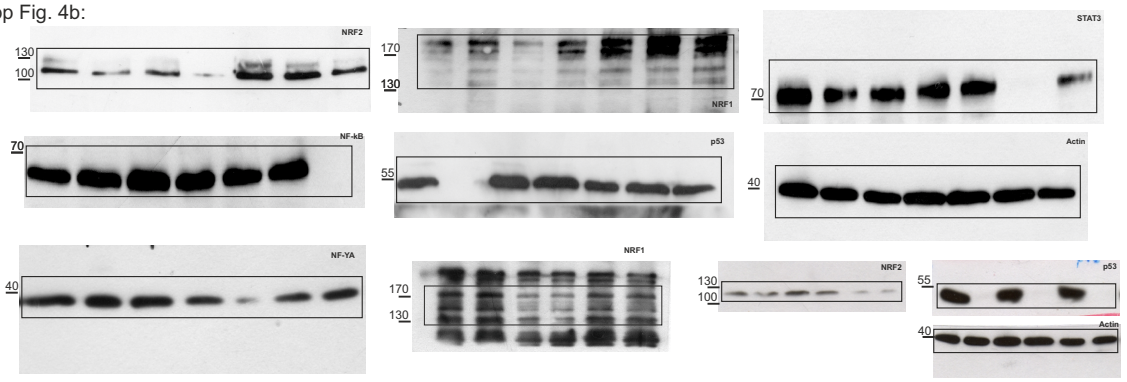

Supp Fig. 4c:

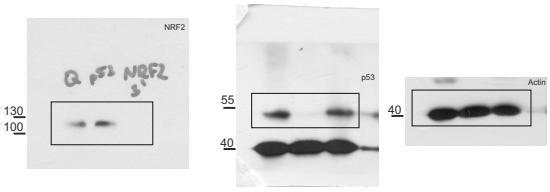

Supp Fig. 5a

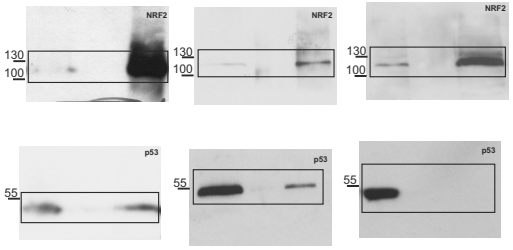

Supp Fig. 5b

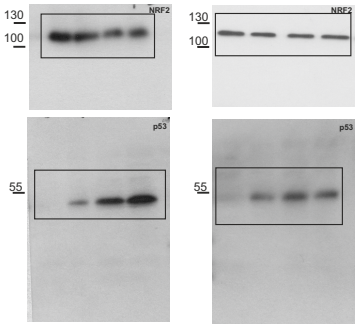

Supp Fig. 5c

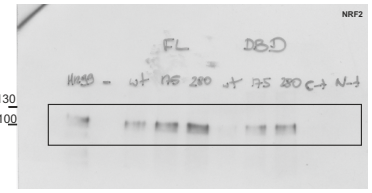

Supp Fig. 5d

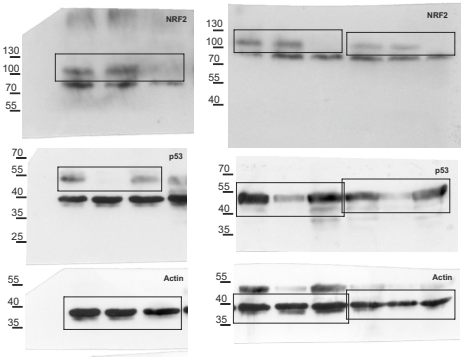

Supp Fig. 5e

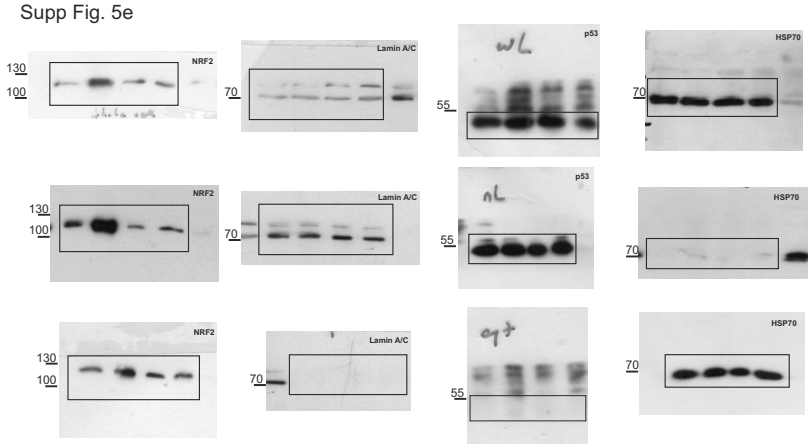

Supp Fig. 5f

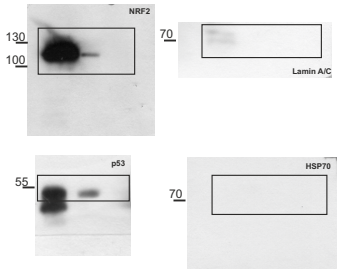

Supplementary Figure 9 continued

Supp Fig. 6a:

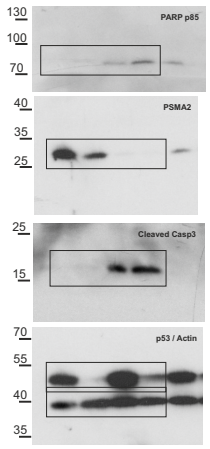

Supp Fig. 6b:

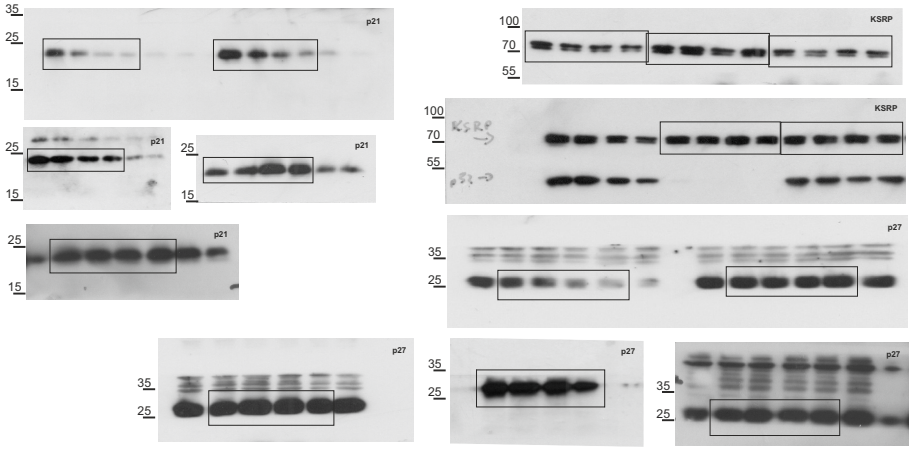

Supp Fig. 6d:

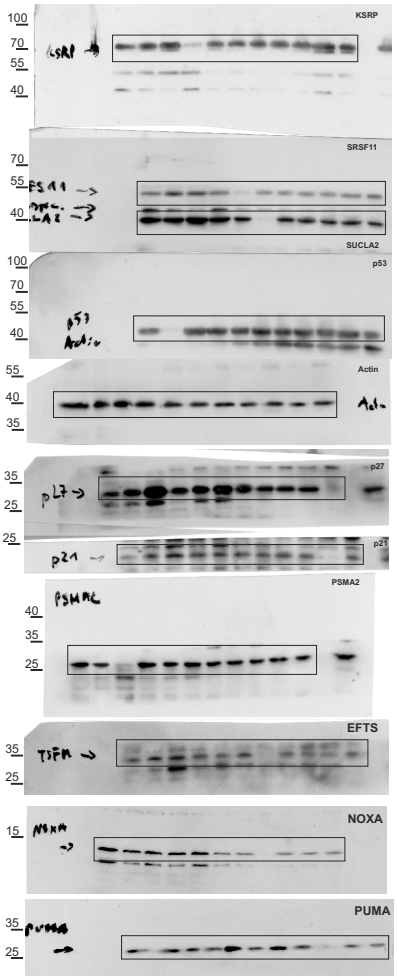

Supp Fig. 6e:

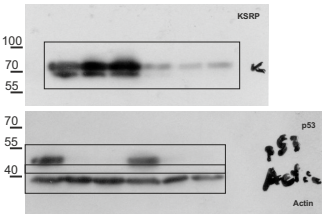

Supp fig.6c

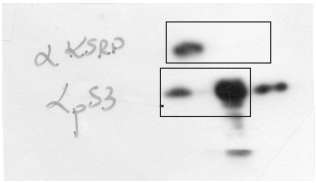

Supp Fig. 6g:

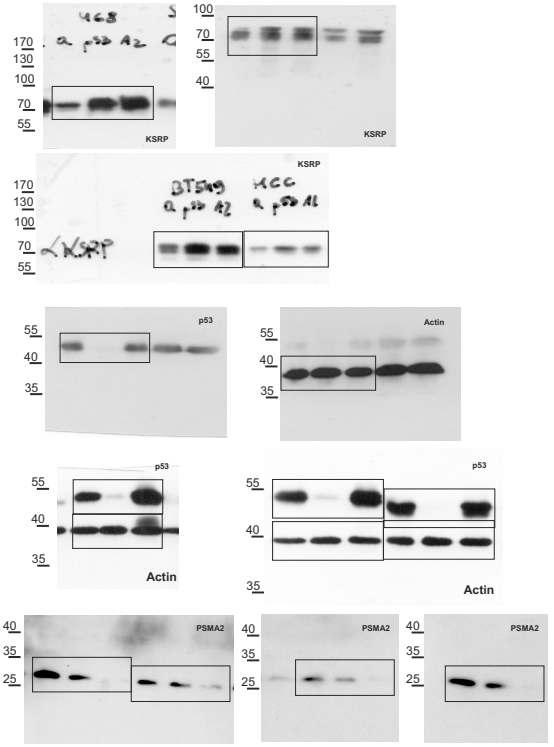

Supplementary Figure 9 continued

Supp. Fig. 7c:

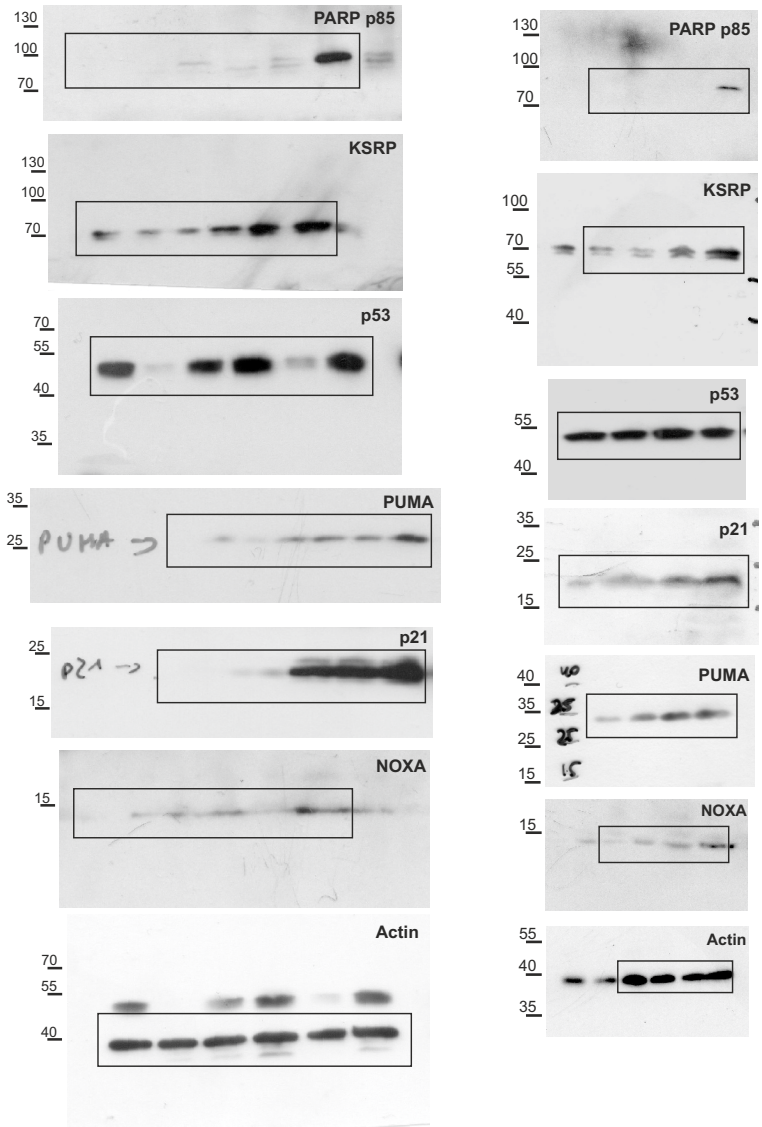

Supplementary Figure 9 continued

Supplementary Tables

Supplementary Table 1 Signatures
Gene and/or protein signatures used for pathway/GO-term, survival and gene status association analyses shown in the study. Integrated, common, mutant p53/proteasome (protein), and cell line-specific mutant p53 expression signatures are shown in worksheet tabs.

Supplementary Table 2 MDA-MB-231 Proteomic analysis
Results of total cell lysate proteomic analyses of MDA-MB-231 cells upon mutant TP53 or PSMA2 silencings (shown in worksheet tabs). Proteins identified by mass-spectrometry across all 8 samples (n=4 controls vs n=4 silencings) in both experiments are listed in the tables and used to calculate fold changes and t-test raw p-values.

Supplementary Table 3 5 TNBC Cell Lines Transcriptomics
Results of transcriptomic analyses in five indicated TNBC cell lines upon mutant TP53 silencing. Transcripts detected in all five experiments are shown (with no additional fold-change or p-value cutoffs applied): RNA-seq for MDA-MB-231 cells and Illumina HumanHT-12-v4-BeadChip for other cell lines. 37 proteasome/immunoproteasome (PSMxy) subunit genes are highlighted in blue.

Supplementary Table 4 MDA-MB-231 ChIPseq Peak Calling
Results of ChIP-sequencing peak-calling in DO-1 anti-p53 IP sample of MDA-MB-231 cells. Fold enrichements, FDRs, closest genes and their transcription start site (TSS) distances are listed for the peaks at indicated chromosome positions (tab 1). List of peaks called at -/+ 500 bp from adjacent gene TSSes (tab 2). Enrichment values for each gene/cell line included in the Fig. 4a low-scale ChIP analysis (tab 3).

Supplementary Table 5 Proteasome Transcripts qPCR
Levels of 37 proteasome/immunoproteasome transcripts in five TNBC cell lines upon silencing of mutant TP53 using two alternative siRNAs (TP53 I and II) in relation to control silencing (tab 1). Levels of 37 proteasome/immunoproteasome transcripts in MDA-MB-231 upon NRF2 silencing in relation to control silencing. Standard deviations (s.d.) are derived form n=2 (tab 2).

Supplementary Table 6 TF identification
Identification of transcription factor binding sites in mutant p53 binding regions in 37 proteasome/immunoproteasome gene promoter regions (based on ChIP-seq results form Supplementary Table 4) as descried in Methods. Transcription factors known to regulate proteasome transcription and analyzed in Fig. 4 are highlighted in yellow.

Supplementary Table 7 Primers and siRNAs
mRNA qPCR primers, ChIP qPCR primers and siRNA sequences used in the work are listed in the in worksheet tabs.

Supplementary Table 8 Feature selection analysis for proteasome signature
Full result of the feature analysis (see Methods) of the 37 genes proteasome/immunoproteasome signature shown in Supplementary Fig. 2c. The 6-gene signature with best score of association with mutant p53 status in breast cancer as well as the full 37 genes signature (with marginally worse result) are highlighted in yellow.

Supplementary Table 9 MDA-MB-231 RNAseq FPKM and Raw counts
FPKMs and Raw Counts for MDA-MB-231 RNA-seq result upon mutant TP53 silencing (n=3) vs control silencing (n=3).

Supplementary Table 10 Statistics Source Data
Data used to calculate statistics in Figs. 1d, 3a, c-f; 4a, 4d-g; 5d; 6e, h-i; 7b and Supplementary Figs. 1e, 3a-c, e-h; 4c-d; 5d,g; 6a,e,h; 7a-b, d-g.

Supplementary Table 11 Antibodies
Antibodies used in the work.

Supplementary Table 12 TNBC Cell Line Characteristics
A table characterizing the TNBC cell lines used for transcriptomic multi-cell line analysis in Figure 1b; contact – missense mutant p53 type influencing p53-promoter DNA contact, conform. - missense mutant p53 type with distorted structure of the p53 DNA-binding domain.

Supplementary Table 13 Signature Pathway Analysis
A table with gene lists and statistical support of top pathways/GO-terms enriched by IPA and ClueGO software analysis of the integrated and common signatures form Fig.1a and b (shown in separate worksheet tabs).
–log (p-value) is derived from Fisher test in IPA; –log (B-H p-value) is derived from Benjamini-Hochberg adjustment of p-values in IPA; Ratio – ratio of associated genes vs all genes in an IPA pathway;
% of As. Genes - percent represented by associated genes in a term in ClueGO; Term Pvalue – p-value of term association in ClueGO; B-H adj Pvalue - Benjamini-Hochberg adjustment of p-values in ClueGO; -log (B-H adj Pvalue) is derived from Benjamini-Hochberg adjustment of p-values in ClueGO.

Supplementary Table 14 TP53 status in TCGA datasets
TP53 status in cancer types used in analysis in Supplementary Fig. 2d. The table cells in grey were selected for analysis as the corresponding cancer types had a balanced mutant TP53 proportion (30%-70%) and number of the validated mutant TP53 samples was above 50. All datasets were derived from the TCGA repository (described in Methods).

Supplementary Table 15 TP53 status of breast cancer patients
Table listing the basal-like primary breast cancer tumor samples from patients, used to determine correlation between the p53 status and the proteasome activity (Fig. 3b). Mutations found by sequencing of the TP53 mRNA expressed in samples are indicated along with the TNBC status, immunohistochemical p53 staining intensity assessment and proteasome chymotrypsin activity measurement result (mean of 3 technical replicates each).